

WIYN Open Cluster Study. XXXIX. Abundances in NGC 6253 from HYDRA Spectroscopy of the Li 6708 Å Region

Barbara J. Anthony-Twarog^{1,3}, Constantine P. Deliyannis^{2,3}, Bruce A. Twarog^{1,3}, Jeffrey D. Cummings^{2,3}, & Ryan M. Maderak²

¹*Department of Physics and Astronomy, University of Kansas, Lawrence, KS 66045-7582*

²*Department of Astronomy, Indiana University, Bloomington, IN 47405-7105*

Electronic mail: bjabat@ku.edu, con@astro.indiana.edu, btwarog@ku.edu, jdcummi@astro.indiana.edu, maderak@astro.indiana.edu

ABSTRACT

High-dispersion spectra of 89 potential members of the old, super-metal-rich open cluster, NGC 6253, have been obtained with the HYDRA multi-object spectrograph. Based upon radial-velocity measurements alone, 47 stars at the turnoff of the cluster color-magnitude diagram (CMD) and 18 giants are identified as potential members. Five turnoff stars exhibit evidence of binarity while proper-motion data eliminates two of the dwarfs as members. The mean cluster radial velocity from probable single-star members is -29.4 ± 1.3 km/sec (sd). A discussion of the current estimates for the cluster reddening, derived independently of potential issues with the *BV* cluster photometry, lead to an adopted reddening of $E(B - V) = 0.22 \pm 0.04$. From equivalent width analyses of 38 probable single-star members near the CMD turnoff, the weighted average abundances are found to be $[\text{Fe}/\text{H}] = +0.43 \pm 0.01$, $[\text{Ni}/\text{H}] = +0.53 \pm 0.02$ and $[\text{Si}/\text{H}] = +0.43_{0.04}^{0.03}$, where the errors refer to the standard errors of the weighted mean. Weak evidence is found for a possible decline in metallicity with increasing luminosity among stars at the turnoff. We discuss the possibility that our turnoff stars have been affected by microscopic diffusion. For 15 probable single-star members among the giants, spectrum synthesis leads to abundances of $+0.46_{0.03}^{0.02}$ for $[\text{Fe}/\text{H}]$. While less than half the age of NGC 6791, NGC 6253 is at least as metal-rich and, within the uncertainties, exhibits the same general abundance pattern as that typified by super-metal-rich dwarfs of the galactic bulge.

Subject headings: open clusters and associations: individual (NGC 6253, NGC 6791) - stars: abundances - techniques: spectroscopic

³Visiting Astronomer, Cerro Tololo Inter-American Observatory. CTIO is operated by AURA, Inc., under contract to the National Science Foundation.

1. INTRODUCTION

Given the amount and level of detailed information potentially available for the local region of the Galaxy, the chemical and dynamical evolution of the Galactic disk offers unrivalled insight into the process of galaxy formation and evolution, at least in the context of generating a well-defined spiral galaxy as the end product. As the database for the population components comprising the Galaxy within the neighborhood of the Sun and beyond has grown in size and precision, the simple picture of Eggen et al. (1962) has given way to a complex evolutionary history increasingly dominated by multiple substructures from within and multiple mergers from without (see, e.g., Prantzos (2008); Freeman (2008); Wyse (2008) among many others). To make sense of these complications, it is valuable to view the Sun and the solar neighborhood within the context of the temporal and spatial evolution of the entire disk. The delineation of that global context requires age, metallicity, and kinematic measures for systems that inhabit zones of the Galaxy well within and well beyond the solar circle. While they can be challenging observationally and their number is modest, open clusters increasingly have been selected as the objects of choice in attempting to probe the history of the Galaxy at large distance and over long periods of time (Bragaglia 2008; Frinchaboy & Majewski 2008). The primary driver behind this trend is the often-noted benefit of being able to derive the age, composition, and distance from collective analysis of the homogeneous cluster stellar sample, rather than from an individual star. The challenges in interpreting the results from the cluster population are often coupled to small samples over a wide range in parameter space (Carraro et al. 1998), a lack of homogeneity in merging the data from different observers applying different approaches (Chen et al. 2003), and the real possibility that subgroups of clusters reflect different origins indicative of the complex structure noted above for field stars (Frinchaboy et al. 2006; Carraro et al. 2006; Warren & Cole 2009).

Among the various properties of the disk that can be probed using open clusters, two primary questions of interest have been the existence of an age-metallicity relation (AMR) (Piatti et al. 1995; Carraro et al. 1998) and the delineation of a radial metallicity gradient (Friel 1995; Twarog et al. 1997; Carraro et al. 1998; Friel et al. 2002; Chen et al. 2003). Once one removes the effect of the latter from the sample, the conclusions regarding the absence of the former have changed little over the last 30 years (Hirshfeld et al. 1978; McClure & Twarog 1978; Friel 1995; Friel et al. 2002). However, the failure to discern an AMR among open clusters may be partly due to the limited age range contained within most cluster samples. Numerous studies over the last few decades have concluded that there is little evidence for a significant change in the mean $[\text{Fe}/\text{H}]$ among stars formed within the solar neighborhood over the last 5-6 Gyrs (Twarog 1980; Meusinger et al. 1991; Edvardsson et al. 1993; Garnett & Kobulnicky 2000; Feltzing et al. 2001; Nordström et al. 2004), though exceptions to this pattern occasionally arise (Rocha-Pinto et al. 2000; Soubiran et al. 2008). Since few clusters survive to this age due to tidal disruption, most cluster-based determinations of the AMR are dominated by samples where no trend is expected, assuming clusters reflect the same history as the field stars. By contrast, if the absence of an AMR over the last 5-6 Gyrs holds throughout the disk, the abundance gradient of the open cluster sample

should be approximately constant with time and, within the statistical uncertainty, should not be dependent upon the mix of ages included within the cluster analysis. As cluster studies extend the temporal and spatial baseline of the sample, the relevance of the objects that populate the extreme ends of the scales becomes an issue of greater concern. For example, the observation that the open cluster sample beyond a galactocentric distance of 10 kpc, on a scale where the Sun is positioned at 8.5 kpc, exhibits, at best, a shallow gradient in metallicity (Twarog et al. 1997) has now been confirmed through the addition of clusters beyond 20 kpc from the galactic center (Yong et al. 2005; Sestito et al. 2008). This immediately raises the question of whether or not the very distant members of this sample are, in fact, representative of the internal development and evolution of the outer Galactic disk or are interlopers accreted via interactions with nearby galactic companions. It should be apparent, however, that this dichotomy may be artificial if the origin and growth of the outer Galactic disk were the products of infalling systems/material from the extended environment of the Galaxy over Gyr timescales (Magrini et al. 2009).

Looking in the opposite direction, cluster studies toward the Galactic center have been hampered by the observational limits imposed by field crowding, high reddening, and a real deficit of surviving clusters interior to a galactocentric radius of 7 kpc. Resulting interpretations of the interior galactic gradient often have been affected by the presence within the sample of perhaps the most anomalous open cluster studied to date, NGC 6791. The extreme nature of the cluster derives from the paradoxical combination of high metallicity and high age, though the degree of the anomaly has remained a point of controversy for decades. A consensus from a variety of studies is that the cluster has an overall metallicity of $[\text{Fe}/\text{H}] = +0.4 \pm 0.1$ based upon intermediate-band photometry (Anthony-Twarog et al. 2007), high resolution spectroscopy of stars in various parts of the CMD, including a horizontal branch star (Peterson & Green 1998), four red giant clump stars (Gratton et al. 2006; Carretta et al. 2007), ten red giant stars (Carraro et al. 2006), and two turn-off stars (Boesgaard et al. 2009), high resolution infrared spectroscopy of six M giants (Origlia et al. 2006), and medium resolution spectroscopy of 24 giants (Worthey & Jowett 2003). Using three different isochrone sets (Demarque et al. 2004; Vandenberg et al. 2006; Pietrinferni et al. 2004), an age of 8 ± 1 Gyr has been determined from isochrone fitting of the cluster turnoff and from the mass-radius diagram of an eclipsing binary (Bedin et al. 2008; Grundahl et al. 2008), though Bedin et al. (2008) derive the puzzling age of 4-6 Gyr from the cooling curve for the cluster white dwarfs.

In most models of galactic chemical evolution, attainment of such a high degree of chemical enrichment within such a short time interval after the formation of the disk presents a significant challenge. Some solutions to the problem have been based upon the unusual kinematics of the cluster, implying that the cluster is either an interloper from a region much closer to the galactic center where a steep linear gradient would indicate the existence of clusters of unusually high metallicity or a cluster captured in a merger event (Carraro et al. 2006). Both interpretations are built upon questionable assumptions tied to the chemical composition of the cluster parent population, particularly the latter solution requiring a super-metal-rich cluster from a dwarf system;

in fact, dwarf galaxies are metal-poor (Skillman et al. 1989; van Zee & Haynes 2006). As long as NGC 6791 represented a unique case, both viewpoints retained some plausibility, but with the discovery of NGC 6253, the picture is significantly altered.

The first comprehensive broad-band photometric study of NGC 6253 was carried out by Bragaglia et al. (1997). Based upon multicolor comparisons to the morphology and luminosity functions of theoretical isochrones, Bragaglia et al. (1997) concluded that the cluster was ~ 3 Gyr old with a metallicity nearly twice solar. From broad-band photometry and integrated spectra, Piatti et al. (1998) found $[\text{Fe}/\text{H}] = +0.2$ and an age of 5 ± 1.5 Gyr. High-dispersion spectra of four giants by Carretta et al. (2000) indicated $[\text{Fe}/\text{H}] = +0.36 \pm 0.15$, a result used by Sagar et al. (2001) to obtain an age of 2.5 ± 0.6 Gyr. A weakness in all these discussions was the exact value of the reddening, which ranged from $E(B - V) = 0.20$ to 0.32 . The first direct measurement of the cluster reddening and metallicity tied to intermediate-band photometry of a large sample of cluster turnoff stars (Twarog et al. 2003) generated $E(B - V) = 0.26 \pm 0.003$, where the error cited is the standard error of the mean (sem), and identified NGC 6253 as the most metal-rich open cluster known, with a metallicity at least as large as NGC 6791 and potentially much larger. A best-fit approach to a match with theoretical isochrones indicated that the cluster CMD morphology was ideally reproduced with an age of 3 ± 0.5 Gyrs and alpha-enhanced isochrones. The weak point in the analysis was the extreme nature of the photometric indices which placed the cluster well beyond the limits of the photometric calibration based upon stars in the solar neighborhood. High-dispersion spectroscopic analysis of 4 clump giants by Carretta et al. (2007) has generated $[\text{Fe}/\text{H}] = +0.46 \pm 0.03$, virtually identical to NGC 6791, while Sestito et al. (2007) find $[\text{Fe}/\text{H}] = +0.36 \pm 0.07$ from 4 probable members. A reanalysis of the intermediate-band photometry of Twarog et al. (2003) using an improved field star calibration (Anthony-Twarog et al. 2007) demonstrated that, independent of the adopted reddening, $[\text{Fe}/\text{H}]$ for NGC 6253 is at least as high as that for NGC 6791 ($[\text{Fe}/\text{H}] = +0.45$) and could be 0.1 dex higher. The most recent addition to the cluster database has been supplied by Montalto et al. (2009), who used a CCD mosaic to measure proper-motion memberships for stars in a large area around the cluster, as well as supplying a new set of *BVR IJHK* photometry. Adopting a low reddening ($E(B - V) = 0.15$) from multicolor fits to theoretical isochrones, Montalto et al. (2009) find a slightly older age (3.5 Gyr) for the cluster than commonly derived, a possible byproduct of comparisons with isochrones that may be too metal-poor ($[\text{Fe}/\text{H}] = +0.22$ and $+0.36$).

While it is clear that, from a chemical composition standpoint, NGC 6253 is a younger cousin of NGC 6791, its extreme characteristics in relation to the rest of the open cluster population and a desire to place it within the context of Galactic chemical evolution make it an important object for study at higher resolution, beyond the handful of clump giants and turnoff stars that have been discussed to date. For this reason, HYDRA spectra of 89 potential cluster members from the tip of the giant branch to below the main sequence turnoff were obtained in multiple wavelength regions for detailed elemental analysis. In this first of three papers we present a discussion of the results for elements other than Li based upon absorption lines in the region of the Li 6708 Å line. Future

papers will discuss other wavelength regions (Maderak et al. 2010), as well as the pattern found for the Li abundance as a function of mass and evolutionary state within the cluster (Cummings et al. 2010).

The layout of the paper is as follows: Sec. 2 presents the observations and their reduction, identification of probable members based upon the derived radial velocities coupled with proper-motion membership, and discussion of the photometric system used to define the stellar colors. Sec. 3 details the determination of the fundamental stellar parameters used in the derivation of the abundances from the absorption lines, Sec. 4 lays out the elemental abundance analysis, and Sec. 5 summarizes our conclusions.

2. SPECTROSCOPIC DATA

2.1. Observations and Reductions

Spectra of 89 stars in NGC 6253 were obtained in 2005, 2006 and 2007 with the Cerro Tololo Inter-American Observatory Blanco 4m telescope equipped with the Hydra multi-object spectrograph. Two distinct configurations were employed in 2005, one (RG/BS) targeting the red giants and blue stragglers of the cluster field, the other (MS/TO) aimed at stars at or below the cluster turnoff. In the Li 6708 Å region, the RG/BS configuration stars received a total of two hours of exposure, all on 19 July 2005. Observations for the fainter, MS/TO configuration stars were obtained in all three years, with the greatest portion of the total signal collected in 2007 due to the poor weather conditions in 2005 and 2006. For the Li region under discussion in this paper, exposures for the MS/TO configuration included 4.4 hours on 18 July, 2005, 12.1 hours on 31 May and 1 June, 2006, and finally 18.5 hours on 25 and 26 May, 2007.

The spectra are characterized by a dispersion of 0.15 Å per pixel in the wavelength range from 6520 Å to 6810 Å with S/N per pixel that ranges from 22 to 127 for the 35 RG/BS stars (2005 data only) and from 30 to 170 for the 54 MS/TO stars. Our signal-to-noise measurements were made by sampling spectra in several spectral regions: from 6680-6690 Å, 6646-6660 Å and 6615-6622 Å. Measurements of S/N per pixel in the 6680-6695 Å region nearer the Li 6708 Å line are higher and will be used in the analysis of the lithium abundances by Cummings et al. (2010). Measured widths for calibration lamp lines from 2005 and 2006 imply a spectral resolution of 15,000 (= 3.0 pixels) in the region near 6700 Å.

Neither configuration utilized the full complement of 132 fibers of the Hydra instrument, leaving dozens of fibers available for measurements of the sky background within the cluster. In practice, low-throughput fibers and the constraints of pre-assigning stellar positions in a crowded field limited the number of fibers usable for sky measurement to approximately 30 fibers, which still provides a significant advantage in determining the local background signal. Prior to the 2007 run, the ThAr lamp became contaminated and unusable; for this set of data, daytime sky spectra were used as

spectral wavelength calibration standards.

The data were reduced using standard reduction routines in IRAF¹. These routines included, in order of application, bias subtraction, division by the averaged flat field, dispersion correction through interpolation of the comparison spectra for data from 2005 and 2006, throughput correction for individual fibers, and continuum normalization. After flat field division and before the dispersion correction, the long-exposure program data were cleaned of cosmic rays using “L. A. Cosmic”². Repeating the procedure for stars observed in NGC 3680 from the 2005 run (Anthony-Twarog et al. 2009), spectra for each star from each night for a given run were combined to produce an annual dataset; a final additive combination of all frames from all years was then generated for the measurement of equivalent widths and the spectral synthesis comparisons.

As mentioned above, due to contamination problems with the normal comparison source, the dispersion corrections for the 2007 spectra were based upon solar/sky spectra taken each afternoon. Comparisons of the final wavelength-defined spectra for NGC 6253 from 2005 and 2006 with the data set from 2007, prior to generating summed spectra from all three runs, proved that the spectra from all three runs were on the same wavelength and zeropoint scale within the resolution-defined uncertainties, i.e. the use of the solar spectra for comparison purposes in 2007 had no significant impact on the radial velocities or the equivalent widths. Moreover, as demonstrated by the test case of NGC 3680 (Anthony-Twarog et al. 2009), our procedures generate equivalent widths and radial velocities that are an excellent match to previous high dispersion studies when a statistically significant sample overlap is available.

2.2. Basic Data: Radial Velocities and Cluster Membership

Because it is the only identification set common to all stars in our sample, stars will be referred to using NGC 6253 identifications on the system of the open cluster database, WEBDA³. Radial-velocity standards were observed on each night of every run to provide an external check on the wavelength calibration and the velocity scale. Individual stellar radial velocities were derived from each annual composite dataset utilizing the fourier-transform, cross-correlation facility FXCOR in IRAF. In this utility, program stars are compared to stellar templates of similar effective temperature (T_{eff}) over the wavelength range from 6575 Å to 6790 Å, as well as a narrower region in the vicinity of H α alone. We have also included in our analysis the radial-velocity measurements obtained in 2007 from spectra in the region of the oxygen triplet (Maderak et al. 2010).

¹IRAF is distributed by the National Optical Astronomy Observatories, which are operated by the Association of Universities for Research in Astronomy, Inc., under cooperative agreement with the National Science Foundation.

²<http://www.astro.yale.edu/dokkum/lacosmic/>, an IRAF script developed by P. van Dokkum (van Dokkum 2001; spectroscopic version).

³<http://www.univie.ac.at/webda>

These radial-velocity measurements were based exclusively on measured wavelengths for lines in the daytime solar spectrum as well as the spectra for program stars.

Even though the 2005 and 2006 data contribute relatively little to the S/N of the combined spectra for the MS/TO stars, these datasets do provide the potential for highlighting radial-velocity variations. With radial velocity (V_r) and rotational velocity information in hand for each annual dataset, our goal was to combine the datasets to produce radial velocities of high internal precision, and then establish the accuracy of the radial-velocity scale with respect to external radial-velocity standards. The first step ensures not only average V_r values of high precision but permits the identification of variable velocity (SB) candidates. The radial-velocity datasets based on spectra in the Li region for 2005 and 2007, as well as the additional dataset from 2007 covering the spectral region of the oxygen triplet, were mapped to the radial velocities of the 2006 dataset in the Li region by determining, then removing, average differences between individual radial velocities in each dataset and the 2006 radial velocities. The four datasets on a common radial-velocity system were combined and averaged; the dispersions associated with the averaged velocities are independent of any uncertainty about the absolute scale of radial velocities, i.e. they remain the same whether one adopts 2006 or any other dataset as the standard.

The immediate benefit is that five candidate spectroscopic binaries with standard deviations above 10 km/sec are easily picked out of the sample of 54 MS/TO stars, as well as seven MS/TO stars with radial velocities that differ from the eventual cluster average by 7 km/sec or more, equivalent to more than five standard deviations, i.e. possible non-members or members within a long-period binary. If these probable SB and/or possible non-members from radial-velocity data alone are excluded, the dispersion among the averaged mean radial velocities for the remaining 42 stars is ~ 1.2 km/sec, quite close to the average error for a single FXCOR measurement, indicating that the averaging process has not introduced significant scatter into the average radial velocities through the inclusion of unrecognized non-members or candidate SB's.

Comparison of the derived and published velocities for our radial-velocity standards suggested the need for a correction to this preliminary average velocity scale; this correction of -1.27 km/sec introduces an added uncertainty in the zero-point of the radial-velocity scale of ± 0.26 km/sec. The added component is included in the standard deviation associated with the average radial velocity for cluster MS/TO members of -29.32 ± 1.30 km/sec or ± 0.2 km/sec (sem). Note that, as discussed below, two of the MS/TO stars classed as members through their radial velocities are probable proper-motion non-members. If these two stars (7638, 7806) with $V_r = -30.23$ and -28.19 km/sec are excluded, the average cluster radial velocity remains unchanged. We will return to the final membership classification using the combined insight from both radial velocities and proper-motions after discussing the RG/BS stars.

A single dataset provides information about the radial velocities for the red giant and blue straggler (RG/BS) candidates observed in 2005. No identification of radial-velocity variability is possible; the radial-velocity scale was adjusted based on comparison to the appropriate night's

radial-velocity standards. For the subset of 18 apparent radial-velocity members, the average cluster velocity is -29.60 ± 1.50 km/sec (sd). Three of the stars excluded from this average (5201, 2542, 2126) are probable members from proper-motion data. One possible blue straggler (5201) has a larger than average uncertainty in V_r ; stars 2542 and 2126 have $V_r = -24.52$ and -37.14 km/sec, respectively, so their inclusion in the average for the evolved stars would lower the mean velocity by 0.12 km/sec. Fig. 1 shows the histogram of radial velocities for the combined RG/BS and MS/TO samples. For the latter, probable binaries have been excluded from the counts; the velocity range used to define cluster membership from radial velocity alone is noted. The average of all probable radial-velocity single members, MS/TO as well as evolved stars, is -29.41 ± 1.31 km/sec (sd) or ± 0.17 (sem).

We can compare our cluster velocity results with two recent studies of NGC 6253. Carretta et al. (2007) studied five red giant stars. One of the five has a velocity of -20.6 km/sec; removing it from the sample produces a tighter average cluster velocity of -28.26 ± 0.6 km/sec (sd) among the remaining four giants. A similar result is obtained by Sestito et al. (2007) from seven stars ranging from the turnoff to the red giant branch clump. A rather noisy average suggests that not all are single and/or member stars; the average of the four most similar velocity values is -29.71 ± 0.79 km/sec (sd).

More specific, star-by-star comparisons are also possible with respect to both of these spectroscopic studies. Three of the five stars studied by Carretta et al. (2007) are within our sample of RG/BS stars. Our velocities are, on average, 0.35 ± 0.46 km/sec lower than those of Carretta et al. (2007) for stars 3595, 2885 and 4510, i.e. not significantly different. Two of the stars studied by Sestito et al. (2007) are within our survey sample, although one of them (2542) is considered a likely non-member in both studies. For the other star, 3138, our velocity is 0.6 km/sec lower, within the individual errors of both surveys.

Of the 89 stars in our sample, 41 have proper-motion membership estimates from Montalto et al. (2009). A plot of the radial-velocity measures, with error bars, for these 41 stars as a function of proper-motion probability is illustrated in Fig. 2. For the final membership classification, any star with a radial velocity that differed from the cluster mean by more than 5.2 km/sec (four standard deviations) was classed as a radial-velocity non-member. Two stars with velocities offset by just under 5.2 km/sec (2542, 5201) are tagged as possible radial-velocity nonmembers. Keeping in mind that proper-motion data are available for only 41 stars in our sample, any star with a probability below 50% was classified as a definite proper-motion non-member. Combining the results from both membership criteria whenever possible, the agreement between the two indicators is excellent. Excluding probable binaries with large radial-velocity dispersions, only four stars are classed as having uncertain final membership, 2542, 5201, 2126, and 7348. Our final designation of membership based upon the combined membership classification is represented in Fig. 2 by circles (probable members), squares (probable non-members), and triangles (uncertain membership).

Table 1 presents the WEBDA identifications, radial-velocity measures, BV photometry from

Twarog et al. (2003) and Montalto et al. (2009), membership based upon radial velocity alone, spectroscopic signal-to-noise per pixel values, proper-motion membership probabilities, and a final overall determination of membership for the 89 stars observed in NGC 6253. Where multi-year observations were available, the dispersion from year-to-year radial velocities is indicated in the error column; for the candidate RG/BS stars, the radial-velocity error from a single observation is indicated.

2.3. Basic Data: Photometry

Photometry from Twarog et al. (2003) has been used as the primary source for $B - V$; the reader is referred to this paper for details on the compilation and merger of the published CCD photometry used to construct the BV catalog. Fig. 3 illustrates the CMD distribution of the stellar sample with filled symbols identifying probable member binary-star candidates. Squares and circles designate stars observed within the RG/BS and MS/TO categorization, respectively; crosses and asterisks are the probable non-members among these two respective categories. Four triangles designate the stars with uncertain membership.

It is important to emphasize that the majority of the MS/TO star candidates were selected for inclusion in the spectroscopic survey primarily on the basis of their identification as probable members through their locations in the CMD, coupled with analysis of the intermediate-band photometry of Twarog et al. (2003). Of the 52 stars tagged as possible members through the photometry, 44 ended up as probable members from both radial-velocities and proper-motions, with only 5 stars classed as likely binaries, an exceptional success rate that indicates the efficiency of the intermediate-band approach for optimizing sample selection among fainter stars in clusters when alternative membership information is lacking.

The $B - V$ data of Twarog et al. (2003) were compiled by converting the observed $b - y$ CCD indices into $B - V$ through a direct comparison to the merged CCD $B - V$ data from three independent sources (Bragaglia et al. 1997; Piatti et al. 1998; Sagar et al. 2001). This approach was taken because the internal errors of the $b - y$ photometry were considerably smaller than most of the quoted errors for the published BV surveys and the $uvby$ study covered a significantly larger field. The average standard errors of the mean for V and $b - y$ for the MS/TO sample are 0.0033 and 0.0048, respectively. The comparable data for the RG/BS stars are 0.0031 and 0.0043, respectively. Transferred into $B - V$, the average standard errors of the mean in color become 0.0083 for MS/TO stars and 0.0063 for the RG/BS stars. The system of Sagar et al. (2001) was selected as the standard because it agreed with that of Piatti et al. (1998), though with better internal errors, and both of these studies showed no color dependence among the residuals in V when compared to the $uvby$ value of V . By contrast, the photometry of Bragaglia et al. (1997) exhibited a significant color term in B when compared to the other sources and a smaller but real color term in V when compared to the V magnitudes from the $uvby$ data. With the CCD mosaic study of NGC 6253 by Montalto et al. (2009) now available, how do the photometric systems

compare?

The data from Montalto et al. (2009) were cross-matched with the stars observed by Twarog et al. (2003) and the residuals in V determined, in the sense (MON - TAD), for approximately 2400 stars brighter than $V = 18.0$. The patterns that emerged are best illustrated using the stars brighter than $V = 16.5$ to minimize confusion caused by the larger sample size and scatter at fainter magnitudes. Fig. 4a shows the residuals as a function of the X-pixel coordinate of the Wide Field Imager, a mosaic of eight 2K x 4K CCDs. (For details regarding the instrumentation, the reader is referred to the discussion by Montalto et al. (2009).) The boundaries of three of the CCD chips within the mosaic array that overlap the *uvby* field in the X-pixel direction are easily identified, as is the discontinuity in residuals for stars on the chip located at X greater than 610 pixels. From 758 stars with X below 610 pixels, the average residual in V is $+0.009 \pm 0.014$ mag (sd); for 168 stars above $X = 610$ pixels, the mean residual is -0.034 ± 0.014 mag. Fig. 4b shows the comparable info for the CCD Y-pixel coordinate direction, where each chip identified in X covers the entire Y direction without a break. The offset created by the pattern in X is obvious. Besides this, there is a small trend in the residuals with Y. Between $Y = -1000$ and $+900$ pixels, the residuals shift by ~ 0.02 mag. Whether this arises from the *uvby* data, the BV data, or both cannot be determined. This level of change is of little consequence and the offset in V at large X is readily corrected, if necessary. The small scatter among the residuals is gratifying and it appears that the V photometry is on the same system at the ± 0.01 mag level. Moreover, if we assume that the dispersion in the V residuals is due to equal contributions by both sources of photometry, the upper limit on the errors in V for the data adopted in this study becomes 0.010 mag. However, we emphasize that for the purposes of this investigation, use of the BV system of Twarog et al. (2003) remains unchanged; V magnitudes and the color-based temperatures discussed in Sec. 3 do not include the photometric data of Montalto et al. (2009).

For the current investigation, the critical question is the B photometry or, equivalently, $B - V$. Unlike V , we cannot use a direct comparison from *uvby* data to test the reliability of the B zero-point or color dependence. We can, however, test for consistency among the four CCD surveys now available. Fig. 5a shows the residuals in $B - V$, in the sense (MON - REF), as a function of $(B - V)_{MON}$ for the photometry of Piatti et al. (1998) (crosses) and Sagar et al. (2001) (open circles). As before, we have restricted the samples to the brighter stars to illustrate the pattern. Confirming the analysis in Twarog et al. (2003), the color dependence of the residuals is the same for both surveys, implying that the Montalto et al. (2009) data are too blue at the cluster turnoff ($(B - V) = 0.8$) by ~ 0.04 mag, with the offset growing to 0.12 mag by $B - V = 1.3$. The analogous comparison for the data of Bragaglia et al. (1997) is shown in Fig. 5b. At the cluster turnoff, the zero-point offset found in Fig. 5a is confirmed. However, the steep color dependence among the residuals is dramatically reduced. This presents us with two possible zero-points for the $B - V$ colors, as defined by the color of the stars at the cluster turnoff, and two options for the differential color of the giant branch relative to the turnoff. For this investigation, we will adopt the BV data of Twarog et al. (2003) as our photometric system and explore the impact of the alternate choices

on our conclusions. In general, a bluer zero-point and/or a smaller differential color between the giant branch and the turnoff will increase our metallicity estimates for the turnoff stars and/or the giants.

3. FUNDAMENTAL STELLAR PARAMETERS

The reliability of the final stellar elemental abundances is dependent in large part upon the accuracy of the stellar parameters that characterize the model atmospheres used in interpreting the measured equivalent widths. Once membership is established, the three primary parameters of interest are the effective temperature, surface gravity, and microturbulent velocity, with different sensitivities to each for giants and dwarfs.

3.1. Reddening and Photometric Temperatures

What is the foreground reddening to NGC 6253? Can we predict the unreddened colors of highly metal-rich stars? These are separate questions with unfortunately intertwined answers, both of which bear upon the larger and more critical issue of effective temperatures based upon photometric colors. Since reddening estimates are often tied to color comparisons to unreddened stars of similar metallicity, it is imperative that a statistically significant sample of minimally reddened field stars be accessible for comparison. At the expected metallicity and effective temperature range of NGC 6253, nearby field stars of appropriate effective temperature are few and far between, requiring the extrapolation of trends from a lower $[\text{Fe}/\text{H}]$ range. However, there is reason to suspect that metallicities well above solar affect optical colors by amounts that exceed the normal extrapolations, a point we will return to below.

A related issue worth considering is whether a helium abundance significantly different from a near-solar value could, by itself, alter the stellar colors appreciably. Girardi et al. (2007) explored this possibility with an explicit reassessment of the effects of helium abundance differences on bolometric corrections and color-temperature relations. Their approach included a recomputation of ATLAS9 models for a range of compositions spanning increments of 0.1 in Y , the helium abundance by mass fraction, and reaching $[\text{Fe}/\text{H}]$ values significantly above solar. Based upon their conclusions, it seems very unlikely that even extreme helium abundance differences would appreciably affect the $(B - V)$ colors for stars approaching the Sun’s surface gravity and effective temperature.

To constrain the cluster reddening while sidestepping the question of the BV photometry, a number of options exist. First, an upper limit on the foreground reddening to NGC 6253 may be set via the dust maps of Schlegel et al. (1998) in the direction of the cluster; $E(B - V) = 0.35$ is found for NGC 6253’s galactic coordinates. However, as discussed in previous papers, given the low galactic latitude of the cluster and the correlated modest distance away from the plane (~ 190 pc), NGC 6253 is probably affected by less than this full amount, although the exact fraction

is unknown. Moreover, Arce et al. (1999) indicate that the reddening maps of Schlegel et al. (1998) overestimate the size of the reddening for estimates above $E(B - V) = 0.15$. If we adopt the relation for adjusting the high-end reddening as determined by Karataş & Schuster (2006), the Schlegel et al. (1998) value for the direction of NGC 6253 is reduced to $E(B - V) = 0.26$.

Second, one can use intermediate-band, $uvbyCaH\beta$ photometry to define the intrinsic colors of the stars near the turnoff under the assumption that the line index, $H\beta$, is metallicity and reddening-independent. Using traditional intrinsic-color relations tied to stars in the solar neighborhood, Twarog et al. (2003) found $E(B - V) = 0.26 \pm 0.003$. Ongoing investigation of the fundamental calibrations of the photometric system for cooler and/or more metal-rich stars (Anthony-Twarog et al. 2002; Twarog et al. 2002, 2007a,b) has demonstrated that, when projected to very high metallicity, the standard intrinsic color relations for cooler dwarfs tend to underestimate the value of the $b - y$ index, leading to an overestimate of the reddening. This implies that $E(B - V) = 0.26$ should be a plausible upper limit for the true reddening value. The size of the metallicity effect has been forcefully demonstrated for NGC 6791 (Anthony-Twarog et al. 2007), where the traditional calibration from intermediate-band analysis led to $E(B - V) = 0.23$, well above the limit imposed by the dust maps of Schlegel et al. (1998). Direct comparison with field stars of comparable effective temperature and metallicity produced a more plausible $E(B - V) = 0.15-0.16$. An attempt to correct the comparable problem for NGC 6253 proved less satisfactory due to the shortage of hotter dwarfs with spectroscopic abundances and intermediate-band photometry at the metallicity derived for NGC 6253. Using an extrapolation from stars slightly more metal-rich than the Hyades, Anthony-Twarog et al. (2007) found $E(B - V) = 0.16$, the same value as NGC 6791, for $[Fe/H] = +0.57$, on a scale where NGC 6791 has $[Fe/H] = +0.45$. If the metallicity of NGC 6253 is closer to that of NGC 6791, the reddening must be higher. We regard the $E(B - V) = 0.16$ estimate as a lower limit to the true cluster value as defined by intermediate-band photometry.

A CMD-based third option is to make use of broad-band IR photometry of giants in the two clusters of comparable metallicity, NGC 6791 and NGC 6253. Following the approach of Carney et al. (2005), we collected JHK magnitudes and colors with the highest quality index from the 2MASS data archive for stars near NGC 6253. Matching the 2MASS positions to the existing photometric survey effectively restricted this search to stars within $6.5'$ of the cluster center. Figure 6 shows an overplot of the $K, (J - K)$ color-magnitude diagram for NGC 6791 (triangles) and NGC 6253 (circles). A color offset of $+0.06$ mag has been applied to the $(J - K)$ colors for the NGC 6791 stars, while a 2.1 mag adjustment has been applied to the fainter NGC 6791 K magnitudes. The alignment of the giant branches and the red clumps of the two clusters suggests that the foreground reddening, $E(J - K)$, for NGC 6253 is at least 0.06 mag larger than that of NGC 6791. The conclusion that this value represents a lower limit results from a presumption that NGC 6253's younger age should result in an intrinsically bluer giant branch with respect to that of NGC 6791. However, the alignment in the JK CMD is set by the assertion that the absolute magnitude and color of the clumps are the same in K and $(J - K)_0$, independent of age, at least

for older clusters. For a complete discussion of this important issue, see Carney et al. (2005). Following Carney et al. (2005), we employ reddening relations from Rieke & Lebofsky (1985) to convert $\Delta E(J - K) \geq 0.06$ to $\Delta E(B - V) \geq 0.12$ with respect to NGC 6791. Using *JHK* analysis, Carney et al. (2005) cite a result of $E(B - V) = 0.14$ for NGC 6791, implying a reddening of at least $E(B - V) = 0.26$ for NGC 6253. As a compromise among the range of potential values, $E(B - V) = 0.22 \pm 0.04$ has been used to correct the NGC 6253 stars for reddening.

For effective temperature estimates for the MS/TO stars and the blue stragglers, we have maintained use of the color-temperature relation developed by Deliyannis and co-workers, as detailed in Anthony-Twarog et al. (2009). We have also compared effective temperatures derived from $(B - V)$ colors to similar results based upon use of the Ramírez & Meléndez (2005) color-temperature relations. For both color-temperature scales, if $[\text{Fe}/\text{H}] = 0.45$ is assumed as characteristic of the cluster stars, the scales are essentially indistinguishable, differing by less than 10 K over the applicable and narrow range of effective temperatures for the turnoff and main sequence stars. For the evolved stars, we converted $(B - V)_0$ to T_{eff} using the color-temperature relation of Ramírez & Meléndez (2005), a revision of the dwarf and giant calibrations of Alonso et al. (1996, 1999). For the effective temperature and gravity range of our red giant stars, the color-temperature relations of Ramírez & Meléndez (2005) produce results essentially identical to the slightly older relations of Alonso et al. (1996, 1999); they are explicitly designed to be applicable to stars as metal-rich as $[\text{Fe}/\text{H}] = 0.5$.

As a test of the consistency of the effective temperature scale for the turnoff stars implied by the adoption of $E(B - V) = 0.22$ and the $B - V$ zero-point of the photometry excluding the data of Montalto et al. (2009), we appealed to the high-dispersion spectroscopic catalog of field stars by Valenti & Fischer (2005), expanded and enhanced in Twarog et al. (2007b, 2009), to compare $H\beta$ indices and spectroscopic temperature estimates for the small sample of catalog stars with $[\text{Fe}/\text{H}] \geq 0.30$. This relationship was applied to the normal sequence defined by turnoff and main sequence stars in NGC 6253 to map effective temperatures to observed $(b - y)$ colors. This mapping relation predicts that turnoff stars characterized by $(b - y) = 0.57 \pm 0.01$ should have effective temperatures of 5935 ± 60 K. This corresponds precisely with the predicted effective temperatures for these stars using the adopted color-temperature calibration with a reddening value of $E(B - V) = 0.23$. Since we have adopted a correction of 0.22 mag to the $(B - V)$ colors in NGC 6253, use of higher reddening would lead to higher derived elemental abundances. Correspondingly, from 34 turnoff members between $B - V = 0.82$ and 0.93, the average difference in $B - V$, in the sense (Table 1 - MON), is 0.039 ± 0.017 mag. Adoption of the Montalto et al. (2009) zero-point for the BV photometry is equivalent to raising the implied reddening for the analysis of stars at the turnoff on our adopted photometric zero-point to $E(B - V) = 0.26$, generating higher abundances for the stars at the turnoff.

Since the colors are used predominantly for the purpose of setting the effective temperature scale, the real question is whether the color shift resulting from the combined effect of the reddening correction and the $B - V$ zero-point leads to correct effective temperatures. If it were possible to

derive the effective temperatures from spectroscopic line analysis, independent of the colors and the reddening, errors in the photometric zero-point would translate into compensating errors in the derived reddening, leaving the color temperature the same as that predicted by the spectroscopic analysis, although in that case, additional errors would be introduced due to the greater dependence of the analysis on the model atmospheres. For reasons discussed below, this approach was only possible for two stars at the turnoff; the derived spectroscopic temperatures were in excellent agreement with those produced from the color calibration with the photometry and reddening as adopted.

How does our effective temperature scale compare with that of previous spectroscopic studies? Turnoff stars have only been observed by Sestito et al. (2007) and neither of their two turnoff stars overlap with our study. However, because our $B - V$ colors for the vertical portion of the turnoff are on the same color system as Bragaglia et al. (1997), we can compare the temperature scales as predicted from our photometry with the photometric scale derived by Sestito et al. (2007). Keeping in mind that Sestito et al. (2007) adopt $E(B - V) = 0.23$, the average photometric temperature for stars 3053 and 2225 is 5937 K using, in their case, the $(B - V) - T_{eff}$ relation for dwarfs from Alonso et al. (1996). Our average photometric temperature for the same stars with our adopted value of $E(B - V) = 0.22$ is 6011 K. Since we are using the same color indices, the offset is entirely a result of the slight change in reddening, our higher adopted value of $[Fe/H]$ within the color- T_{eff} relation, and use of the revised color- T_{eff} relation. More important from the standpoint of the final abundance determinations, the average effective temperature for these two stars derived by Sestito et al. (2007) from spectroscopy, independent of the reddening and used in the abundance analysis by Sestito et al. (2007), is 6125 K. Sestito et al. (2007) estimate an upper limit to the uncertainty in their spectroscopic temperatures of ± 70 K. Therefore, were we to derive our abundances for the turnoff stars using the spectroscopic effective temperature scale of Sestito et al. (2007), our abundances would increase. The exact size of the change will be dealt with in Sec. 4.

For the giants, our samples overlap with two stars, 2542 and 3138. As one might expect given that our $B - V$ system for the giants is 0.065 mag redder and that we adopted a reddening value that is 0.01 mag smaller, the difference in the photometric temperatures, in the sense (Table 4 - SES), averages -80 ± 14 K for Sestito et al. (2007), i.e., our temperatures are cooler. The analogous offset with the spectroscopically derived effective temperatures is -34 ± 6 K, implying that our current abundances for the giants are only slightly less than or equal to what they would be if we had used the spectroscopic effective temperature scale of Sestito et al. (2007).

By contrast, the effective temperatures of Carretta et al. (2007) are purely photometric and are based upon $V - K$, bypassing the concern raised by the B photometry. Adopting $E(B - V) = 0.23$, the average difference in the photometric temperatures, in the sense (Table 4 - CAR), from three giants in common is 147 ± 34 K, implying that, relative to Carretta et al. (2007), the spectroscopic and photometric scales of Sestito et al. (2007) are too hot by 180 K and 227 K, respectively; the estimated uncertainty in the temperatures of the giants as derived by Carretta et al. (2007) is

± 70 K. The temperature difference goes the wrong way in that it implies that our adopted $B - V$ colors are too blue. Obviously, if the abundances of Carretta et al. (2007) were derived using our photometric temperature scale or either effective temperature scale of Sestito et al. (2007), their metallicities for the giants would increase, but exactly how much depends upon any correlated effects of altering the microturbulent velocity and the surface gravity, a point we will return to in Sec. 4.

3.2. Surface Gravity and Microturbulent Velocity

Another necessary input parameter for our spectroscopic analysis is a surface gravity estimate for each star. Without an extensive list of measured lines of different ionization states, we were unable to determine $\log g$ from the spectra alone. Instead we tested the isochrones of Chaboyer and collaborators (Dotter et al. 2008) and the Yale-Yonsei (Y^2) isochrones (Demarque et al. 2004) to supply an appropriate set for a match to the abundance and age of NGC 6253. Scaled-solar isochrones for $[\text{Fe}/\text{H}] = 0.45$ were obtained from the web interface for the Dartmouth Stellar Evolution (DSE) database (stellar.dartmouth.edu/~models/index.html) and the Y^2 web site (<http://www.astro.yale.edu/demarque/yyiso.html>). With $[\text{Fe}/\text{H}]$ and $E(B - V)$ fixed, only the distance modulus remains as a free parameter. Optimal matches were determined by eye, with special emphasis on the turnoff region and subgiant branch luminosity due to the inconsistency of the colors of the isochrone giant branches for any plausible age estimate. For DSE, an isochrone with an age of 3.3 Gyr matches the turnoff and subgiant branch of NGC 6253 reasonably well for an assumed reddening $E(B - V) = 0.22$ and apparent distance modulus of $(m - M) = 12.0$, but fails to reproduce the colors and magnitude of the giant branch and giant branch clump; more specifically, while the isochrone values for $\log g$ for the clump giants correspond to an expected value of ~ 2.5 , the isochrone effective temperatures are generally 200 K cooler than indicated by photometric color-temperature relations. By contrast, the Y^2 isochrones with an age of 3.0 Gyr and an apparent modulus of 11.9 provide the optimal match to the cluster with $E(B - V) = 0.22$. The predicted giant branch is also redder than the cluster, but by a significantly smaller amount than the DSE comparison. The comparison for Y^2 is illustrated in Figure 7, in which scaled-solar isochrones with $[\text{Fe}/\text{H}] = 0.45$ have been adjusted by an apparent distance modulus of 11.9 and $E(B - V) = 0.22$ and compared to photometry compiled by Twarog et al. (2003). The ages of the presented isochrones are 2.6, 3.0 and 3.4 Gyr.

A simple match of V magnitudes to $\log g$ values from the fitted isochrones sufficed for main sequence, turnoff and subgiant branch stars; the two independent isochrone sets agreed in $\log g$ at the ± 0.03 level, a difference too small to impact the final abundances. Because of the failure of both sets of isochrones to superpose upon the observed giant branch, the giant branch stars clearly needed a different approach. In the DSE isochrones for this high metallicity, the surface gravity of the clump stars increases gradually from $\log g = 2.5$ at ages below 3 Gyr to values near 2.6 for ages above 4.5 Gyrs. A value of 2.55 was chosen as the representative surface gravity for stars

populating the red giant branch clump in NGC 6253. The V magnitudes for the giant branch stars were artificially offset to force a match between the magnitude of the cluster’s red giant branch clump to the comparable feature in the isochrones at $\log g = 2.55$, i.e. the surface gravities were derived differentially relative to the clump luminosity.

Microturbulent velocities (V_t) for F and G dwarfs are commonly estimated from a formula developed by Edvardsson et al. (1993) which depends on effective temperature and surface gravity. Previous spectroscopic analyses by the Indiana group have used this formula exclusively, but its development did not include stars with metallicities as high as those found in NGC 6253. An ideal transformation of measured line equivalent widths into abundances uses the 2002 version of the local thermodynamic equilibrium (LTE) line analysis/spectrum synthesis code MOOG (Snedden 1973) and appropriate stellar atmospheres. It is possible, in principle, to determine the optimum effective temperature and microturbulent velocity by minimizing the trend of derived abundances as functions of excitation potential and equivalent width for different lines. In practice, most of the spectra produced indeterminate results with this approach; finding “clean” lines in spectra this metal-rich is a challenge. For only two stars among the MS/TO stars, 4375 and 2193, was it possible to independently arrive at effective temperature and microturbulent velocity estimates. Based upon the implied microturbulent velocities for these two stars, V_t values from the Edvardsson et al. (1993) formulation appeared to be too large by 0.2 km/sec and 1.1 km/sec. For the present analysis, the intercept of the Edvardsson et al. (1993) relation for microturbulent velocities was reduced by 0.8 km/sec, a weighted average of the individual offsets, retaining 0.8 km/sec as a minimum value. The sensitivity of $[\text{Fe}/\text{H}]$ to microturbulent velocity implies that the derived $[\text{Fe}/\text{H}]$ values are boosted by ~ 0.2 dex by this adoption of a lower V_t scale in the analysis of the equivalent widths among the dwarfs.

As a modest check on our approach, we note that in their discussion of stars near the main sequence turnoff Sestito et al. (2007) derived microturbulent velocities from analysis of the spectra, finding a microturbulent velocity of 1.27 km/sec for the one probable member, 3053. The prescription from Edvardsson et al. (1993) would predict a microturbulent velocity nearly 1.0 km/sec higher, using their derived effective temperature and estimated surface gravity.

The recipe for microturbulent velocities among dwarf stars cannot be applied to giants. Based upon extensive analyses of open cluster giants by the Indiana group using similar spectra (see, e.g. Jacobson et al. (2009) and references therein) we set the microturbulent velocity scale for the clump stars to a value of 1.5 km/sec. For evolved stars brighter (fainter) than the clump, the gravity-dependent formula of Carretta et al. (2004) was used to increment (decrement) V_t through a differential comparison to the $\log g$ of the clump stars.

4. ELEMENTAL ABUNDANCE DETERMINATION

4.1. Dwarf Abundances - Fe, Si, Ca, Ni

The determination of elemental abundances in NGC 6253’s candidate MS/TO stars began with the adoption of a list of cleanly measurable iron lines used in common with other cluster investigations by the authors within the Indiana University group, an approach that should enhance the consistency with other cluster results generated from the same procedure. The very strong lines in the spectra for NGC 6253 members, however, made adherence to this original line list difficult. To identify alternative lines as replacements for the iron lines that were crowded by nearby strong lines, we synthesized predicted equivalent widths for lines in linelists generated from atomic data made available by Kurucz⁴ using MOOG and an atmospheric model with characteristics similar to our turnoff stars. All model atmospheres were generated from the Kurucz (1992) model atmosphere set for specified T_{eff} , $\log g$, microturbulent velocity and input abundance. Our final linelist consisted of 15 iron lines, to which three measurable lines of neutral Ni (6643, 6768 and 6772 Å) and one line each for Si (6721 Å) and Ca (6717 Å) were added.

Equivalent widths were measured using the IRAF routine SPLIT, then processed using the force-fit abundance routine *abfind* in MOOG. An estimated error for each equivalent width measurement was made using a formula described by Deliyannis et al. (1993) using the width of the line and the S/N ratio per pixel. For a spectrum with a S/N per pixel of 100, the error in the equivalent width is approximately 5 mÅ. These steps were replicated for 20 separate exposures of the solar spectrum obtained from our daytime sky exposures from the 2007 run, adopting an effective temperature of 5770 K, surface gravity of $\log g = 4.40$ and a microturbulent velocity of 1.14 km/sec for the Sun. Signal-to-noise per pixel values for these solar spectra ranged from 102 to 195. All resulting stellar abundances were differenced with respect to the generated solar abundances on a line-by-line basis. This minimizes the impact of the specific choice of $\log gf$ values on the final abundances from the individual lines. All measured equivalent widths for the 38 probable member MS/TO stars are listed in Table 2, available in full form in the on-line edition of the journal.

Table 3 presents [Fe/H] estimates for each of 38 probable member dwarfs, based on 9 to 15 iron lines per star. For elements with multiple lines, the standard error of the mean abundance is presented; for elements with single lines, the error presented has been propagated from the formal error in the equivalent width measurement. Table 1 includes 40 single probable members among the MS/TO sample. The spectrum for the very faintest star, 7822, could not be measured with any degree of security. Another star, 2562, was included in the observing configuration composed of MS/TO stars but sits at the base of the red giant branch, and will be included with the red giant sample. Some individual equivalent width measurements were discarded in the course of analysis: equivalent widths less than 15 mÅ (approximately 3 times the typical error in equivalent width) or greater than 200 mÅ, for which a line would be considered strong, as well as the few measures with

⁴<http://cfaku5.cfa.harvard.edu/linelists.html>

calculated formal errors in the equivalent width that were comparable to the EW measurement.

A histogram of individual iron abundance measures was constructed for all lines and all member stars in the MS/TO sample, following which measures of $\log A(\text{Fe})$ below 7.4 and above 8.5 were excluded (corresponding to $[\text{Fe}/\text{H}]$ above 1.0 or below -0.1). All individual values of $\log A(\text{Fe})$ were converted to a linear scale before averaging; the logarithmic abundance was recreated following an averaging procedure weighted by individual measurement errors. From 38 turnoff members, the weighted average abundances are found to be 0.43 ± 0.01 , 0.53 ± 0.02 , 0.43 ± 0.03 and 0.61 ± 0.02 for $[\text{Fe}/\text{H}]$, $[\text{Ni}/\text{H}]$, $[\text{Si}/\text{H}]$, and $[\text{Ca}/\text{H}]$, respectively. The errors refer to the standard error of a weighted mean; because we averaged the numerical abundances rather than the logarithmic quantities, the resulting errors are asymmetric. We note that for abundance estimates covering a realistically large range, the order of computational operation is critical; the consequence of averaging logarithmic abundances would be an estimated average $[\text{Fe}/\text{H}]$ nearly 0.1 dex lower over our large sample of abundances from 504 iron lines.

Figures 8 and 9 provide representative illustrations of the lack of a significant dependence of the derived iron abundances on V magnitude and on wavelength, where the plotted abundance is the appropriate average for each MS/TO star in Figure 8, for each line in Figure 9. Errors shown in both figures are standard deviations. A linear fit through the data in Fig. 8 does indicate a weak dependence (slope of 0.08 ± 0.03 with a correlation coefficient of 0.42) of the abundance on position within the vertical turnoff with the stars at $V = 14.75$ ending up 0.15 dex more metal-poor than stars at $V = 16.5$. The statistical significance of the slope is rather marginal, making it difficult to know whether this is a real effect tied to physical processes occurring in the outer layers of stars, or whether this is a byproduct of our reduction procedure. Keeping this caveat in mind, one might wonder whether we have detected the effects of microscopic diffusion, however marginally.

4.2. Evidence for Microscopic Diffusion?

Microscopic diffusion can affect the elemental abundances observed on stellar surfaces. The efficiency of convective mixing wipes out any diffusion that might have occurred inside a convection zone; however, gravitational settling and thermal diffusion can drain elements out of the *bottom* of the surface convection zone (SCZ), and thus reduce the surface abundance. Conversely, radiative levitation can push elements into the SCZ, thereby enriching the surface abundances (e.g. Michaud (1986)). The efficiency of downward diffusion generally increases toward the surface, so cooler dwarfs with deeper SCZs should suffer the least diffusion, while progressively hotter dwarfs (with shallower SCZs) should show progressively more diffusion, and stars near the turnoff should show the most. Deepening SCZs during subgiant and giant evolution would erase diffusion-related surface abundance anomalies created during the main sequence, either by dredge-up of material diffused downward during the main sequence (Deliyannis et al. 1990), or by dilution of radiative levitation-enhanced turnoff surface abundances. Some evidence exists for downward diffusion in turnoff stars of the very metal-poor globular cluster M92 (King et al. 1998; Boesgaard et al.

1998; Ramírez et al. 2001; Korn et al. 2007) but Gratton et al. (2001) find no differences between turnoff stars and giants in the somewhat more metal-rich globulars NGC 6397 and NGC 6752, although Korn et al. (2007) claim that such differences do exist in NGC 6397. Richard et al. (2002) studied the metallicity dependence of diffusion in models spanning $[\text{Fe}/\text{H}] = -4.3$ to -0.7 , and argued that the most metal-poor turnoffs would show the greatest amount of diffusion, due in part to the fact that increasing metallicity results in cooler turnoff T_{eff} at a given age. Thus, it could very well be the case that only the most metal-poor globulars, such as M92, will show significant differences between the turnoff and the RGB.

Michaud et al. (2004) constructed stellar evolutionary models that included diffusion for solar-metallicity stars, with particular application to the old open clusters M67 and NGC 188. (We are not aware of any diffusion models for super-metal-rich stars such as those of NGC 6253.) They assumed turnoff T_{eff} of about 6150 K and 5950 K, respectively, which are close to our turnoff T_{eff} for NGC 6253 of about 6000 K; recall also that NGC 6253 could easily be a little hotter or cooler (Sec. 3.1). Near the turnoff, the degree of diffusion becomes a steep function of T_{eff} : for example, for the M67 models, Fe has diffused (downward) by 0.04 dex at 6000 K but by over 0.08 dex near 6100 K (see their Fig. 2). Just past the turnoff, the abundance- T_{eff} relation loops even as dredge-up begins because the SCZ is shallower as compared to the depth of a pre-turnoff dwarf of the same T_{eff} (see also Deliyannis et al. (1990)). The abundance continues to rise with further evolution, and reaches the initial model value by the base of the RGB. (There is slightly less diffusion in the cooler turnoff models of NGC 188, as compared to the turnoff of M67, and it should be kept in mind that slow mixing, for example, as induced by rotation, can inhibit diffusive motions; see also Sills & Deliyannis (2000); Deliyannis et al. (1998).)

It should be stressed that the super-metal-rich turnoff/dwarf stars of NGC 6253 are expected to be more massive than those in M67 (at a given T_{eff}), which may lead to different diffusion model predictions. Nonetheless, the above predictions are consistent with our observations of Fe in NGC 6253. As discussed above, the cluster Fe abundances seem to decrease from the coolest (faintest) dwarfs near $V = 16.5$ up to the turnoff, by of order 0.1 dex or so, though the Fe- V slope is significant at only the 2.7σ level (and could be an artifact of the reduction procedures). Undeterred by the lackluster statistical support of this argument, we can attempt to examine the data even more closely. It is tempting to conclude that most of the slope is indeed seen in Fig. 8 where predicted, namely from $V = 16.5$ up to the top of the purely vertical part of the main sequence at $V = 15.3$. Above this, stars become slightly cooler (up to $V = 15.0$), where there is somewhat of a turnoff gap (up to about $V = 14.6$), and then we see the very hottest *subgiants*. The model predictions are complex in this region (see the bottom of the Fe- T_{eff} curve in Fig. 2 of Michaud et al. (2004)), with clear dredge-up in the cooler subgiant models. This is not inconsistent with our Fe data from $V = 15.3$ to 14.5, including the seemingly higher Fe abundances in our brightest two stars, although the error bars are also consistent with no real scatter. Finally, although our average $[\text{Fe}/\text{H}]$ of $+0.46_{-0.03}^{+0.02}$ for the giants (see Sec. 4.3) is within the errors of our value of $+0.43 \pm 0.01$, for the dwarfs, a small difference between the two, as perhaps predicted by diffusion, is possible.

In short, our data are not inconsistent with diffusion, and are even slightly suggestive of its effects, but with only a weak statistical significance, at best.

It is interesting to point out that, although the metallicities reported in the various studies of NGC 6791 (see Sec. 1) essentially agree to within the errors, the lowest reported spectroscopic value comes from the two turnoff stars of Boesgaard et al. (2009); all other values are higher, and are from stars in more advanced stages of stellar evolution.

4.3. Giant Abundances - Fe

We approached the abundance determinations for the giant stars somewhat differently for a number of reasons. First, while our target selection among the MS/TO candidate stars was optimized by photometry to exclude non-members, the configuration involving brighter stars (giants, subgiants, potential blue stragglers) was designed to include any plausible candidate in the field. As a result, the fraction of non-members is higher. Perhaps more important, due to the high metallicity we expected spectra for the evolved stars to be at least as difficult to interpret as the MS/TO stars; tests with synthetic spectra confirmed that continuum placement would be challenging for the giant branch stars. Following Carretta et al. (2007), we selected seven spectral regions surrounding iron lines for synthesis. Linelists were constructed using the online linelists of Kurucz focussed narrowly around the following iron lines: 6646, 6703, 6733, 6608/9, 6725/6, 6750/2 Å. In addition, a 30 Å region around the Li 6708 Å line was synthesized and compared with observed spectra. For each member on the giant or subgiant branch at or below the level of the red giant branch clump, model atmospheres with the adopted effective temperature, $\log g$ and microturbulent velocity were constructed for iron abundances ranging in 0.05 dex increments from 0.1 to 0.5, then compared by eye to the observed spectrum within the MOOG software suite. The iron abundance reported in Table 4 represents an average of the determinations from each separate wavelength region as determined by two separate measurers. The quoted error is the standard deviation. For the fourteen stars analyzed, the average of $[\text{Fe}/\text{H}]$ values is +0.46 with a standard deviation of 0.03 (0.01 sem). We have been careful to maintain a distinction between averages of $[\text{Fe}/\text{H}]$ values, as opposed to averaging non-logarithmic estimates of iron abundance; the logarithms of the average iron abundance yield an indistinguishable result for the representative average abundance of $+0.46_{-0.03}^{+0.02}(\text{sd})$.

Several probable non-members with CMD positions near the red giant branch clump also were analyzed in a similar way. If non-members, the assumptions leading to the adopted effective temperatures of the models would be incorrect. If, as is likely, the reddening correction is too large for foreground non-members, comparison to synthetic spectra with effective temperatures that are too high would lead to an over-estimate of the iron abundance. Abundances of $[\text{Fe}/\text{H}]$ for these five stars range from 0.19 to 0.31, systematically lower than found among the probable single-star members and consistent with an even lower abundance field population overcorrected for reddening.

4.4. Abundance Errors

Systematic or random errors among any of several parametric decisions will lead to abundance errors. For MS/TO stars, the dependencies of $[\text{Fe}/\text{H}]$ on errors in surface gravity, effective temperature and microturbulent velocity were determined by exploring a grid of models used to analyze the measured equivalent width data, specifically the data for star 7292 in the vertical turnoff region typifying the MS/TO sample. In summary, the effects on $[\text{Fe}/\text{H}]$ due to changes in T_{eff} of +100 K, in $\log g$ of 1.0, and in V_t of -1.0 km/sec are found to be 0.08, 0.09, and 0.28 respectively. A comparable exploration of model parameters for stars at the bright and faint end of the giant branch members supplies comparable sensitivities of 0.03, 0.18 and 0.46 respectively, indicating even more modest sensitivity to temperature estimates but enhanced sensitivity to surface gravity and especially microturbulent velocity estimates.

For comparison, both Sestito et al. (2007) and Carretta et al. (2007) present detailed explorations of the effects of parameter choices on their derived abundances. In summary, the effect on the $[\text{Fe}/\text{H}]$ of a red giant branch star resulting from changes of +100 K in effective temperature and of -1.0 km/sec for microturbulent velocity are +0.02 and +0.42, respectively, similar to the sensitivities in our abundances for comparable stars. Examination of the effect of changing parameters on $[\text{Fe}/\text{H}]$ for the MS/TO stars by Sestito et al. (2007) may be compared with our results as follows: the effect on $[\text{Fe}/\text{H}]$ of a +100 K change in effective temperature is +0.07 dex, while a change -1.0 km/sec in V_t generates a shift of +0.30 dex in $[\text{Fe}/\text{H}]$.

With the derived dependencies of $[\text{Fe}/\text{H}]$ on each of our model parameters, it should be possible to estimate the systematic effect of different reddening or photometric zero-points; these dependencies may also be used to estimate the propagated effect of random photometric errors, if the forms of our color-temperature relation and formulation for V_t may be assumed to be correct. The precision of V and $(B - V)$ values for individual stars is 0.0031 mag and 0.0063 mag, respectively, for RG/BS stars and 0.0033 mag and 0.0083 mag, respectively, for MS/TO stars based upon the original photometry (Twarog et al. 2003). As discussed in Sec. 2.3., comparison to the photometry of Montalto et al. (2009) places a probable upper limit of 0.010 mag on the errors in V . A similar comparison in $B - V$ leads to a probable upper limit to the errors of 0.012 mag.

For MS/TO stars, the surface gravities may be determined with a precision of ± 0.05 from isochrone comparisons, so the sensitivity to surface gravity uncertainties is negligible; for completeness, an error of 0.0033 mag in V translates into a random error of 0.001 in $\log g$. A random error in $(B - V)$ of 0.0083 maps to a random error in temperature of 27 K. Collectively, these affect V_t at the level of 0.022 km/sec. Combined in quadrature, these random errors imply a dispersion in $[\text{Fe}/\text{H}]$ of ± 0.023 . If we adopt the upper limits for the representative errors (0.010 mag and 0.012 mag in V and $(B - V)$), the corresponding numbers for $\log g$, T_{eff} , V_t , and $[\text{Fe}/\text{H}]$ become 0.003, 39 K, 0.032 km/sec and 0.033 dex, respectively.

For the giants, V_t depends only on $\log g$, which again depends only on the V magnitude. A random color error of 0.0063 mag folds into an error in T_{eff} of 12 K for the adopted color- T_{eff}

calibration. The effect on the $\log g$ estimate due to the error in V is 0.002 in $\log g$. In turn, this has an even smaller effect on V_t of 0.00026 km/sec. Collectively, these produce a random error in $[\text{Fe}/\text{H}]$ below 0.01 dex. Raising the adopted uncertainties to 0.01 mag in V and 0.012 mag in $(B - V)$ still leaves the random propagated error in $[\text{Fe}/\text{H}]$ at the 0.01 dex level.

4.5. Comparison to Previous Work

Abundance estimates from the present work may be compared directly to recent high dispersion spectroscopic studies by Carretta et al. (2007) and Sestito et al. (2007). The former study employs spectrum synthesis and a sample of giant stars to arrive at an $[\text{Fe}/\text{H}]$ estimate for the cluster of +0.46. In contrast, Sestito et al. (2007) explore a broader range of stellar type while using measured equivalent widths and abundances referenced to the sun, techniques similar to those employed in our study. Both of these studies analyze high signal-to-noise spectra (~ 100) of higher resolution ($\sim 45,000$) than our dataset; both studies adopt a reddening value for NGC 6253 of $E(B - V) = 0.23$, similar to the value employed here. Differences in adopted values for $\log g$ were very minor and will not be addressed here.

A more detailed comparison to the results of Carretta et al. (2007) indicates some differences that belie the apparent similarity of their abundance result to ours. As noted earlier, from three of the probable member giants that are common to our survey, the effective temperatures adopted by Carretta et al. (2007) are ~ 150 K cooler than ours; their prescription for estimating microturbulent velocities leads to estimates ~ 0.35 km/sec lower than ours. Because the impacts of these two parameters on $[\text{Fe}/\text{H}]$ shift in opposite senses, these choices partly offset each other in $[\text{Fe}/\text{H}]$. To facilitate a comparison of results, we will artificially adjust our abundance estimate in accordance with their parameter selection precepts; such an adjustment raises our average $[\text{Fe}/\text{H}]$ estimate to $[\text{Fe}/\text{H}] = +0.58$.

Comparison of our result to that of Sestito et al. (2007) is complicated by various factors despite the apparent similarity of our approaches: abundances from equivalent widths within the MOOG framework referenced directly to solar spectra. None of the seven stars in the Sestito et al. (2007) sample approaches the unevolved main sequence; of the two stars near the main sequence turnoff, one (2225) appears to be a non-member or SB candidate based upon its radial velocity. Additionally, as the authors themselves conclude, measuring equivalent widths in these highly metal-rich spectra is difficult enough for higher gravity stars, and extremely challenging for the giants. A potential complication is their inclusion of two apparent non-members among the sample of five evolved stars. Our radial velocities for 2542 and 3138 confirm the questionable membership of the former but indicate probable membership for the latter. Based on proper motions, both stars are probable members.

Sestito et al. (2007) estimate effective temperature and microturbulent velocity from their spectra. For the one probable member near the main sequence turnoff, their derived effective

temperature is higher than our color-temperature estimation scheme would predict by ~ 100 K. Since the microturbulent velocity found for this star is lower than our estimation scheme would predict by ~ 0.25 km/sec, if we had adopted the temperature and microturbulent velocity derived by Sestito et al. (2007) for this star, our derived abundance for this star would increase from $[\text{Fe}/\text{H}] = +0.45$ to $+0.59$. For the red giants, Sestito et al. (2007) employ very similar effective temperatures to ours but, again, lower microturbulent velocities. If our abundances are rederived using the parameter estimates of Sestito et al. (2007), our abundances for these stars would be higher by 0.14 dex, or $[\text{Fe}/\text{H}] = +0.60$.

Several comments can be made about these comparisons. Sestito et al. (2007) revise their own abundance estimates for two stars downward by 0.1 dex following a re-examination of several spectra using spectrum synthesis rather than equivalent widths. To counter what appears to be a suggestion that synthesis produces lower abundances than equivalent width analysis, we offer the observation that both types of analysis were attempted for a star at the base of the red giant branch, star 2562. Colors, surface gravity and microturbulent velocities were assigned to this star following the procedures outlined for giant branch and clump stars. The S/N per pixel for the spectra is not high, resulting in a much larger than usual dispersion among the separate line indicators of iron abundance. Despite these issues, the line analysis of 14 lines produced $[\text{Fe}/\text{H}] = +0.48_{0.20}^{0.07}$ (sem), while spectrum synthesis led to $[\text{Fe}/\text{H}] = 0.42 \pm 0.08$. On the basis of this one comparison star bridging the gravity range between the clump and turnoff stars, we can't provide any support for a methodological difference in abundance results for synthesis as compared to equivalent width measurements.

Finally, we reiterate the important effect of averaging logarithmic abundances, as opposed to taking logarithms of abundance numbers. Particularly if the individual abundances include substantial scatter, averaging logarithmic values underestimates the more correct logarithm of the average numerical abundance; for our data the effect was 0.09 dex. The former practice is quite common; had we employed it, the average abundance for the large sample of MS/TO members would be 0.09 dex lower and more consistent with published results in the cluster once differences in parameter selections are accounted for.

5. Summary and Conclusions

High-dispersion spectra centered on the Li line of 89 potential members of the old open cluster NGC 6253 have been processed and analyzed, generating 65 probable radial-velocity members, including 47 dwarfs and 18 red giants. When coupled with recently published proper-motion memberships, the member sample is reduced to 45 dwarfs and 18 red giants. Excluding potential binaries and spectra with inadequate S/N per pixel, abundances have been derived from line analysis for 38 stars at the turnoff and from spectrum synthesis for 15 red giants, with impressive agreement between the two samples for the key element, Fe. For the adopted reddening ($E(B - V) = 0.22$) and effective temperature scale, the mean cluster metallicity lies at $[\text{Fe}/\text{H}] = +0.45$, confirming

previous work from intermediate-band photometry of turnoff stars and high-dispersion analyses of a handful of mostly red giants that placed NGC 6253 among the most metal-rich systems known in the Galaxy, if not the most metal-rich. The issues dogging any discussion of the metallicity of this object bear a strong similarity to those surrounding NGC 6791 - the exact value of the reddening, the appropriate color and effective temperature scale, and an embarrassing richness of lines that can confuse the interpretation of spectra more than enlighten. Despite these caveats, the choices made in setting the cluster parameters have been selected such that probable changes would raise our metallicity determination for NGC 6253. On an absolute scale, if the effective temperature and microturbulence scales had been set using the approaches found in previous high-dispersion work, our NGC 6253 metallicity would be increased by ~ 0.1 dex.

We have presented results for three elements other than iron from the wavelength region around the lithium line. In spite of a very limited linelist, we have recovered essentially solar values for $[A/Fe]$ for nickel and silicon. The implied abundance for $[Ca/Fe]$ is surprising and at variance with the results of Carretta et al. (2007) and Sestito et al. (2007), both of whom recover an essentially scaled-solar abundance for calcium. Our Ca abundance results rest entirely on a single line at 6717 Å. In contrast, both studies from 2007 employ a wider spectral region including 6 lines for the Carretta et al. (2007) study and 22 for the Sestito et al. (2007) work. A direct comparison of measured equivalent widths for MS/TO stars in our study to published equivalent widths for the 6717 Å line indicates that our equivalent width measurements are consistent with those of Sestito et al. (2007), implying that our measurement procedures are not faulty but that the line itself might be seriously contaminated. To test this possibility, equivalent widths were synthesized using MOOG for a solar model and a model typical of the MS/TO region’s parameters in NGC 6253. For the solar model, the 6717 Å line includes a blended feature from Ti II that contributes less than 8% to the effective equivalent width of the line. For the NGC 6253 turnoff star, however, the Ti II line accounts for a 20% contamination of the line feature. A quick correction to the equivalent width to “remove” the contamination from the Ti II line suggests an estimate for $[Ca/H]$ that is nearly 0.3 dex lower, consistent with an essentially scaled-solar abundance for calcium relative to iron.

While additional elements, including O, will be the focus of an analysis of a different wavelength region (Maderak et al. 2010), the pattern emerging from all high-dispersion work done to date is that NGC 6253, like NGC 6791 (Carraro et al. 2006; Origlia et al. 2006; Carretta et al. 2007; Boesgaard et al. 2009), exhibits approximately scaled-solar abundances for a majority of the elements. Note that for NGC 6791, the only element that shows statistically significant deviations from a scaled-solar ratio in multiple analyses is C (Origlia et al. 2006; Carretta et al. 2007); other elements such as Ba and Ni may show deviations in one study, but not in another, or worse, deviations in the opposite sense. As noted by Boesgaard et al. (2009), the pattern of roughly scaled-solar abundance ratios is consistent within the errors with what is observed among very metal-rich field dwarfs found in the solar neighborhood with kinematics that imply a potential origin near the galactic bulge (Pompéia et al. 2002), as well as among probable bulge dwarfs stud-

ied *in situ* through spectroscopy obtained during gravitational lensing events (Cohen et al. 2009). If a link exists between the bulge and NGC 6253, it will need to await additional observational evidence before becoming apparent.

The authors wish to thank the staff at Cerro Tololo Inter-American Observatory for their invaluable assistance in obtaining the observations that form the basis of this study. CTIO is operated by the Association of Universities for Research in Astronomy, under contract with the National Science Foundation. The discussion was greatly enhanced by the photometric and proper-motion data made available by Dr. Montalto and his colleagues. Extensive use was made of the SIMBAD database, operating at CDS, Strasbourg, France and the WEBDA database maintained at the University of Vienna, Austria (<http://www.univie.ac.at/webda>). CPD gratefully acknowledges support from the National Science Foundation under grant AST-0607567. BJAT and BAT are also grateful to the Astronomy Department at Indiana University for hospitality during our Fall 2008 stay and to the University of Kansas for sabbatical support. We all appreciate the thoughtful comments of the referee which improved the paper.

REFERENCES

- Alonso, R., Arribas, R., & Martínez-Roger, C. 1996, *A&AS*, 117, 227
- Alonso, R., Arribas, R., & Martínez-Roger, C. 1999, *A&AS*, 140, 261
- Anthony-Twarog, B. J., Deliyannis, C. P., Twarog, B. A., Croxall, K. V., & Cummings, J. D. 2009, *AJ*, 138, 1171
- Anthony-Twarog, B. J., Twarog, B. A., & Mayer, L. 2007, *AJ*, 133, 1585
- Anthony-Twarog, B. J., Twarog, B. A., & Yu, J. 2002, *AJ*, 124, 389
- Arce, H. G., & Goodman, A. A. 1999, *ApJ*, 512, L135
- Bedin, L. R., King, I. R., Anderson, J., Piotto, G., Salaris, M., Cassisi, S., & Serenelli, A. 2008, *ApJ*, 678, 1279
- Boesgaard, A. M., Deliyannis, C. P., Stephens, A., & King, J. R. 1998, *ApJ*, 493, 206
- Boesgaard, A. M., Jensen, E. E. C., & Deliyannis, C. P. 2009, *AJ*, 137, 4949
- Bragaglia, A. 2008, *MemSAI*, 79, 365
- Bragaglia, A., Tessecini, G., Tosi, M., Marconi, G., & Munari, U. 1997, *MNRAS*, 284, 477
- Carney, B. W., Lee, J.-W. & Dodson, B. 2005, *AJ*, 129, 656
- Carraro, G., Ng, Y. K., & Portinari, L. 1998, *MNRAS*, 296, 145

- Carraro, G., Villanova, S., Demarque, P., McSwain, M. V., Piotto, G., & Bedin, L. R. 2006, *ApJ*, 643, 1151
- Carretta, E., Bragaglia, A., & Gratton, R. G. 2007, *A&A*, 473, 129
- Carretta, E., Bragaglia, A., Tosi, M., & Marconi, G. 2000, in *ASP Conf. Ser. 198, Stellar Clusters and Associations: Convection, Rotation, and Dynamos*, ed. R. Pallavicini, G. Micela, & S. Sciortino (San Francisco: ASP), 273
- Carretta, E., Bragaglia, A., Gratton, R. G., & Tosi, M. 2004, *A&A*, 422, 991
- Chen L., Hou J. L., & Wang J. J. 2003, *AJ*, 125, 1397
- Cohen, J. G., Thompson, I. B., Sumi, T., Bond, I., Gould, A., Johnson, J. A., Huang, W., & Burley, G. 2009, *ApJ*, in press
- Cummings, J. D., Anthony-Twarog, B. J., Deliyannis, C. P., Maderak, R. M., & Twarog, B. A. 2010, *AJ*, in prep.
- Deliyannis, C. P., Pinsonneault, M. H., & Duncan, D. K. 1993, *ApJ*, 414, 740
- Deliyannis, C. P., Boesgaard, A. M., Stephens, A., King, J. R., Vogt, S. S., & Keane, M. J. 1998, *ApJ*, 498, L147
- Deliyannis, C. P., Demarque, P., & Kawaler, S. D. 1990, *ApJS*, 73, 21
- Demarque, P., Woo, J. -H., Kim, Y. -C., & Yi, S. K. 2004, *ApJS*, 155, 667 (Y^2)
- Dotter, A., Chaboyer, B., Jevremovic, D., Kostov, V., Baron, E., & Ferguson, J. W. 2008, *ApJS*, 178, 79 (DSE)
- Edvardsson, B., Anderson, J., Gustafsson, B., Lambert, D. L., Nissen, P. E., & Tomkin, J. 1993, *A&A*, 275,101
- Eggen, O. J., Lynden-Bell, D., & Sandage, A. R. 1962, *ApJ*, 136, 748
- Feltzing, S., Holmberg, J., & Hurley, J. R. 2001, *A&A*, 377, 911
- Freeman, K. C. 2008, in *ASP Conf. Ser. 396, Formation and Evolution of Galaxy Disks*, ed. J. G. Funes, S.J., & E. M. Corsini (San Francisco: ASP), 3
- Friel, E. D. 1995, *ARA&A*, 33, 381
- Friel, E. D., Janes, K. A., Tavaréz, M., Scott, J., Katsanis, R., Lotz, J., Hong, L., & Miller, N. 2002, *AJ*, 124, 2693
- Frinchaboy, P. M., & Majewski, S. R. 2008, *AJ*, 136, 118

- Frinchaboy, P. M., Muoz, R. R., Phelps, R. L., Majewski, S. R., & Kunkel, W. E. 2006, *AJ*, 131, 922
- Garnett, D. R., & Kobulnicky, H. A. 2000, *ApJ*, 532, 1192
- Girardi, L., Castelli, F., Bertelli, G. & Nasi, E. 2007, *A&A*, 468, 657
- Gratton, R. G. et al. 2001, *A&A*, 369, 87
- Gratton, R., Bragaglia, A., Carretta, E., & Tosi, M. 2006, *AJ*, 642, 462
- Grundahl, F., Clausen, J. V., Hardis, S., & Frandsen, S. 2008, *A&A*, 492, 171
- Hirshfeld, A., McClure, R. D., & Twarog, B. A. 1978, in *IAU Symp. 80, The HR Diagram: The 100th Anniversary of Henry Norris Russell*, ed. A. G. Davis Philip & D. S. Hayes (Boston: D. Reidel), 163
- Jacobson, H. R., Friel, E. D., and Pilachowski, C. A. 2009, *AJ*, 137, 4753
- Karataş, Y., & Schuster, W. J. 2006, *MNRAS*, 371, 1793
- Kurucz, R. L., 1992, in *IAU Symp. 149, The Stellar Populations of Galaxies*, ed. B. Barbuy & A. Renzini (Dordrecht: Kluwer), p. 225.
- King, J. R., Stephens, A., Boesgaard, A. M., & Deliyannis, C. P. 1998, *AJ*, 115, 666
- Korn, A. J., Grundahl, F., Richard, O., Mashonkina, L., Barklem, P. S., Collet, R., Gustafsson, B., & Piskunov, N. 2007, *ApJ*, 671, 402
- Maderak, R. M., Anthony-Twarog, B. J., Cummings, J. D., Deliyannis, C. P., & Twarog, B. A. 2010, *AJ*, in prep.
- Magrini, L., Sestito, P., Randich, S., & Galli, D. 2009, *A&A*, 494, 95
- McClure, R. D., & Twarog, B. A. 1978, in *IAU Coll. 45, Chemical and Dynamical Evolution of our Galaxy*, ed. E. Basinska-Grzesik & M. Mayor (Sauverny: Geneva Observatory), 193
- Meusinger, H., Stecklum, B., & Reimann, H.-G. 1991, *A&A*, 245, 57
- Michaud, G. 1986, *ApJ*, 302, 650
- Michaud, G., Richard, O., Richer, J., & Vandenberg, D. 2004, *ApJ*, 606, 452
- Montalto, M., Piotto, G., Desidera, S., Platais, I., Carraro, G., Momany, Y., De Marchi, F., & Recio-Blanco, A. 2009, *A&A*, 511, 1129
- Nordström, B., Mayor, M., Andersen, J., Holmberg, J., Pont, F., Jørgensen, B. R., Olsen, E. H., Udry, S., & Mowlavi, N. 2004, *A&A*, 418, 989

- Origlia, L., Valenti, E., Rich, R. M., & Ferraro, F. R. 2006, *ApJ*, 646, 499
- Peterson, R. C. & Green, E. M. 1998, *ApJ*, 502, L39
- Piatti, A. E., Claría, J. J., & Abadi, M. G. 1995, *AJ*, 110, 2813
- Piatti, A. E., Claría, J. J., Bica, E., Geisler, D., & Minniti, D. 1998, *AJ*, 116, 801
- Pietrinferni, A., Cassisi, S., Salaris, M., & Castelli, F. 2004, *ApJ*, 612, 168
- Pompéia, L., Barbuy, B., & Grenon, M. 2002, *ApJ*, 566, 845
- Prantzos, N. 2008, in *IAU Symp. 254, The Galaxy Disk in Cosmological Context*, ed. J. Andersen et al., arXiv:0809.2507
- Ramírez, S. V., Cohen, J. G., Buss, J., & Briley, M. M. 2001, *AJ*, 122, 1429
- Ramírez, I. & Meléndez, J. 2005, *ApJ*, 626, 465
- Richard, O., Michaud, G., & Richer, J. 2002, *ApJ*, 580, 1110
- Rieke, G. H. & Lebofsky, M. J. 1985, *ApJ*, 288, 618
- Rocha-Pinto, H. J., Maciel, W. J., Scalo, J., & Flynn, C. 2000, *A&A*, 358, 850
- Sagar, R., Munari, U., & de Boer, K. S. 2001, *MNRAS*, 327, 23
- Schlegel, D., Finkbeiner, D. P. & Davis, M. 1998, *ApJ*, 500, 525
- Sestito, P., Randich, S., & Bragaglia, A. 2007, *A&A*, 465, 185
- Sestito, P., Bragaglia, A., Randich, S., Pallavicini, R., Andrievsky, S. M., & Korotin, S. A. 2008, *A&A*, 488, 943
- Sills, A., & Deliyannis, C. P. 2000, *ApJ*, 544, 944
- Skillman, E. D., Kennicutt, R. C., & Hodge, P. W. 1989, *ApJ*, 347, 875
- Snedden, C. 1973, *ApJ*, 184, 839
- Soubiran, C., Bienaymé, O., Mishenina, T. V., & Kovtyukh, V. V. 2008, *A&A*, 480, 91
- Twarog, B. A. 1980, *ApJ*, 242, 242
- Twarog, B. A., Anthony-Twarog, B. J., Feldt, J. A., Liebst, K. A., Mayer, L., & Vargas, L. C. 2007a, *BAAS*, 39, 925
- Twarog, B. A., Anthony-Twarog, B. J., & De Lee, N. 2003, *AJ*, 125, 1383
- Twarog, B. A., Anthony-Twarog, B. J., & Edgington-Giordano, F. 2009, *PASP*, 121, 1312

- Twarog, B. A., Anthony-Twarog, B. J., & Tanner, D. 2002, *AJ*, 123, 715
- Twarog, B. A., Ashman, K. M., & Anthony-Twarog, B. J. 1997, *AJ*, 114, 2556
- Twarog, B. A., Vargas, L. C., & Anthony-Twarog, B. J. 2007b, *AJ*, 134, 1777
- Warren, S. R., & Cole, A. A. 2009, *MNRAS*, 393, 272
- Valenti, J. A., & Fischer, D. A. 2005, *ApJS*, 159, 141
- VandenBerg, D. A., Bergbusch, P. A., & Dowler, P. D. 2006, *ApJS*, 162, 375
- van Zee, L. & Haynes, M. P. 2006, *ApJ*, 636, 214
- Worthey, G. & Jowett, K. J. 2003, *PASP*, 115, 96
- Wyse, R. F. G. 2008, in *ASP Conf. Ser. 399, Panoramic Views of Galaxy Formation and Evolution*, ed. T. Kodama, T. Yamada, & K. Aoki (San Francisco: ASP), 445
- Yong, D., Carney, B. W., & Teixeira de Almeida, M. L. 2005, *AJ*, 130, 597

Fig. 1.— Radial-velocity distribution for the stars in Table 1. The thick solid line identifies the velocity range selected for radial-velocity probable members.

Fig. 2.— Radial velocity as a function of proper-motion membership probability for the stars in Table 1. Circles are stars tagged as likely single star members from the combined information. Squares are probable non-members or long period binaries, while triangles indicate stars with uncertain membership.

Fig. 3.— CMD for the stars included in the current study - Table 1. Circles are MS/TO candidate stars; filled symbols are probable binaries and asterisks are non-members. Squares are RG/BS candidate stars; open symbols are members and crosses are probable non-members. Open triangles are stars with uncertain membership.

Fig. 4.— (a) Residuals in V , in the sense (MON - TAD), for stars brighter than $V_{MON} = 16.5$ as a function of the X-coordinate position in WEBDA pixel coordinates. (b) Residuals in V , in the sense (MON - TAD), for stars brighter than $V_{MON} = 16.5$ as a function of the Y-coordinate position in WEBDA pixel coordinates.

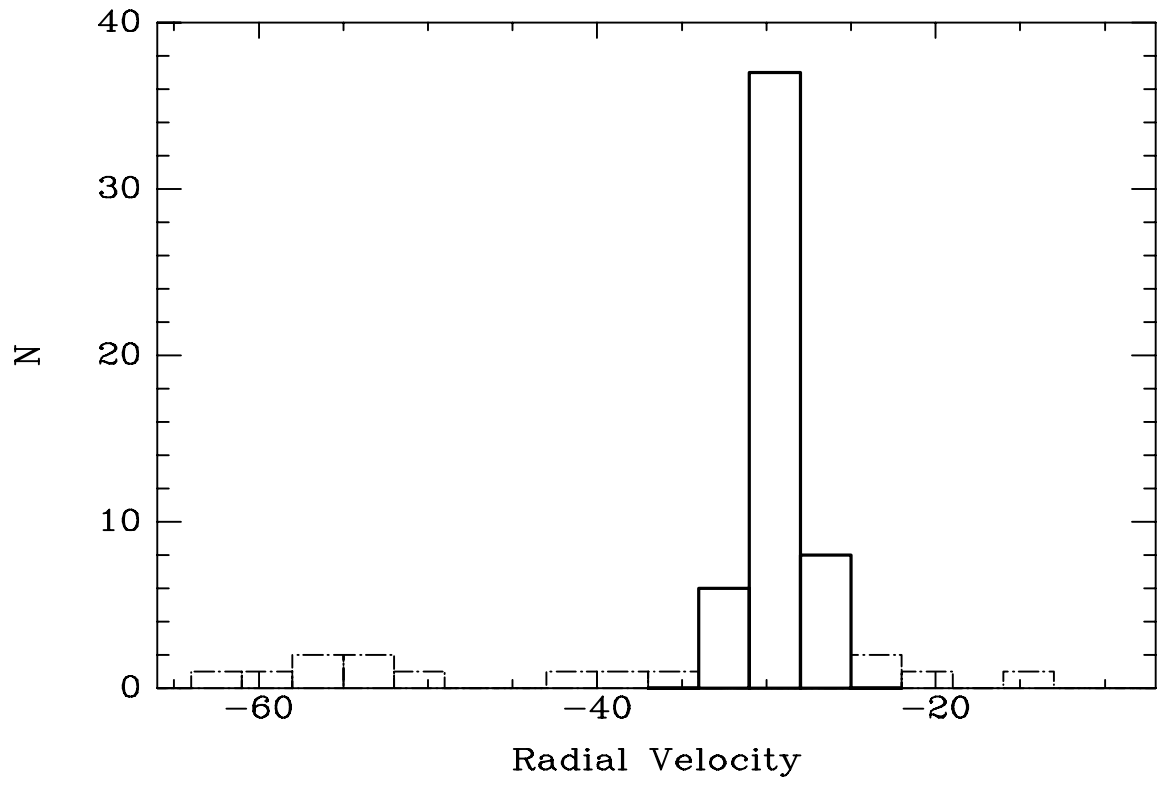
Fig. 5.— (a) The residuals in $B - V$, in the sense (MON - REF), as a function of $(B - V)_{MON}$ for the photometry of Piatti et al. (1998) (crosses) and Sagar et al. (2001) (open circles). (b) Same as Fig. 5a for the data of Bragaglia et al. (1997).

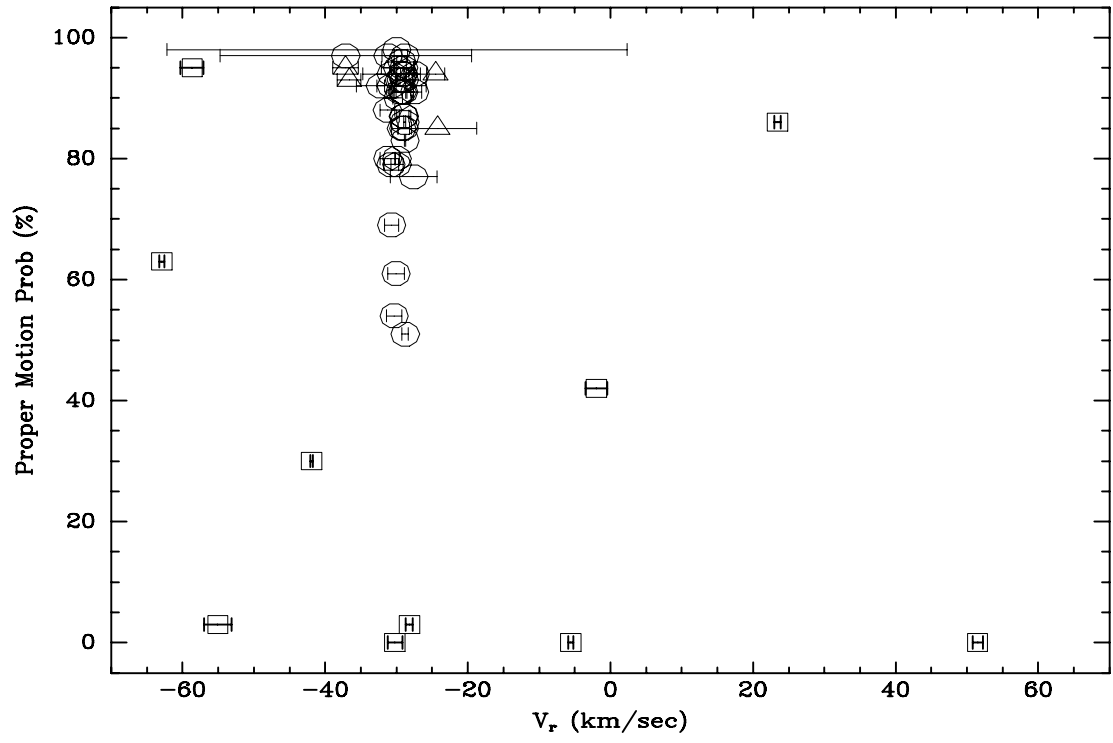
Fig. 6.— The JK CMD for stars in NGC 6791 (triangles) and NGC 6253 (circles). Giants in NGC 6791 have been shifted to the reddening and distance of NGC 6253 by applying offsets of $\Delta(J - K) = +0.06$ mag and $\Delta M_K = -2.1$ mag to the individual points.

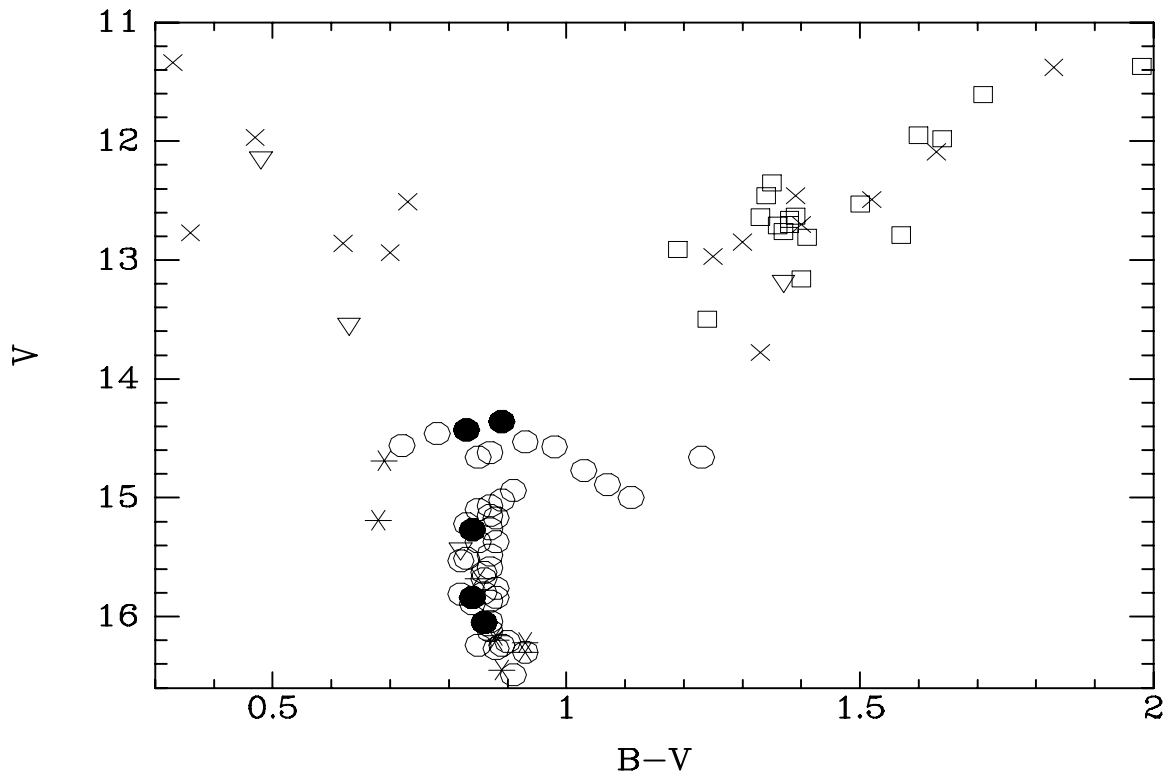
Fig. 7.— Comparison of BV photometry for NGC 6253, compiled by Twarog et al. (2003), to isochrones from Y^2 . Isochrones with a scaled-solar composition of have been adjusted for the apparent distance modulus of the cluster, $\mu = 11.9$ and the adopted reddening $E(B - V) = 0.22$. Isochrones with ages 2.6, 3.0 and 3.4 Gyr are shown.

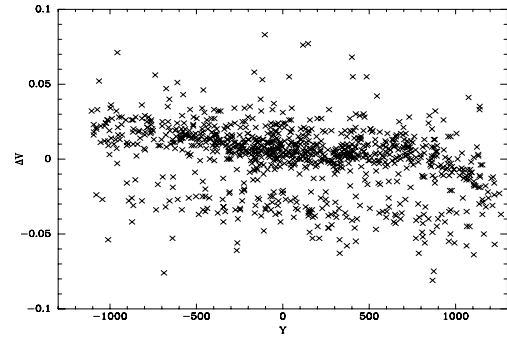
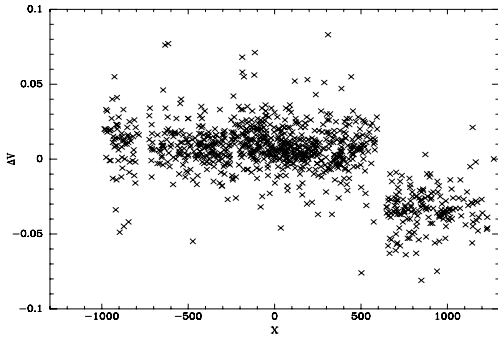
Fig. 8.— Average Fe abundance for each MS/TO star as a function of the V magnitude. Errors bars are the standard deviations in Fe for a given star.

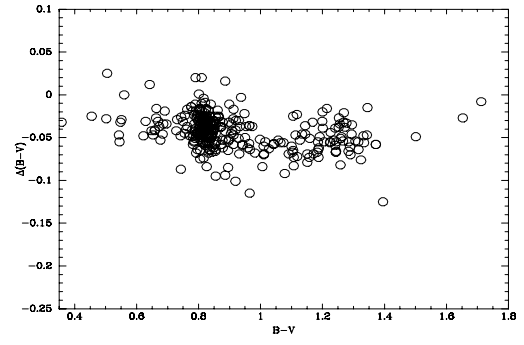
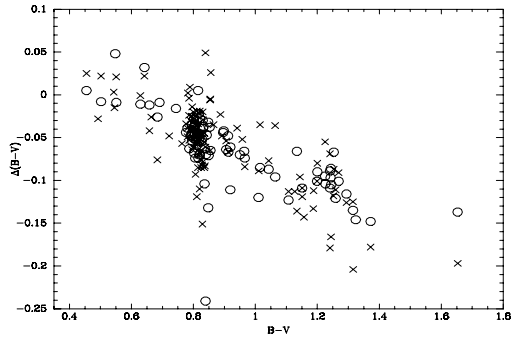
Fig. 9.— Average Fe abundance among the MS/TO stars as a function of the wavelength of the line used to determine the abundance. Error bars are the standard deviation in Fe among the stars for a given line.

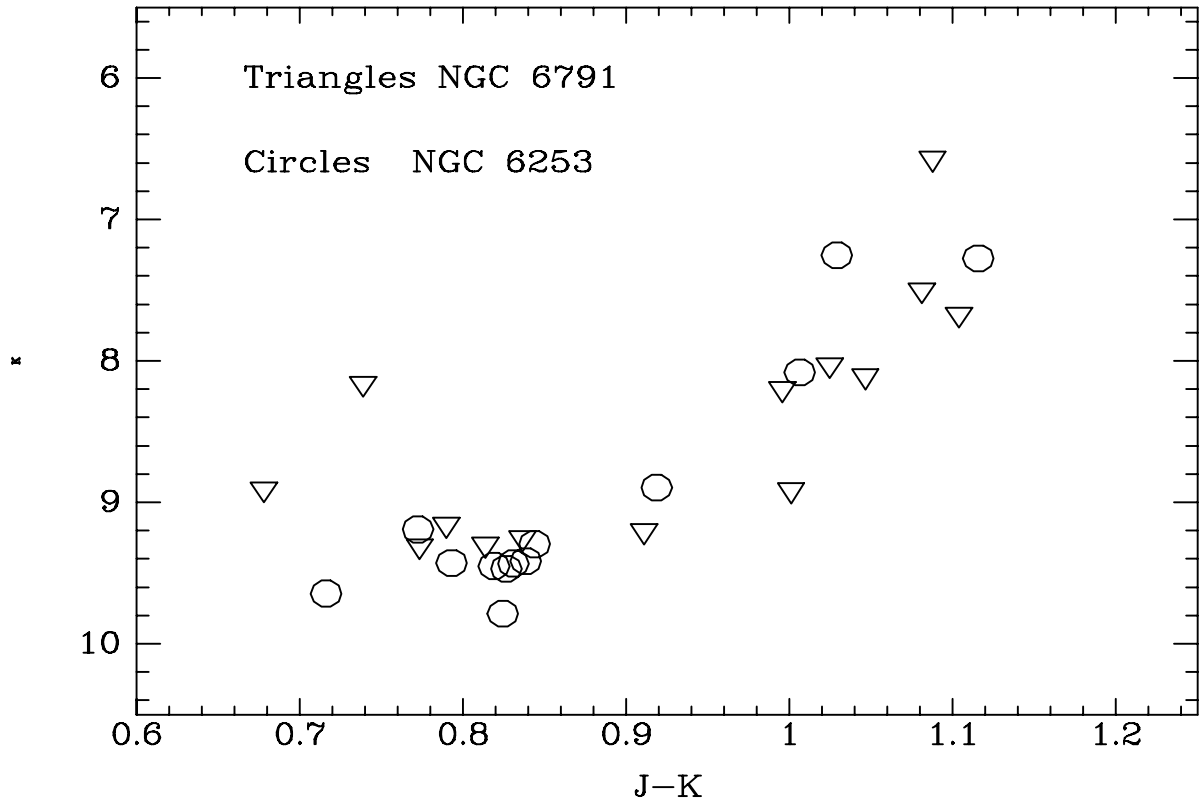


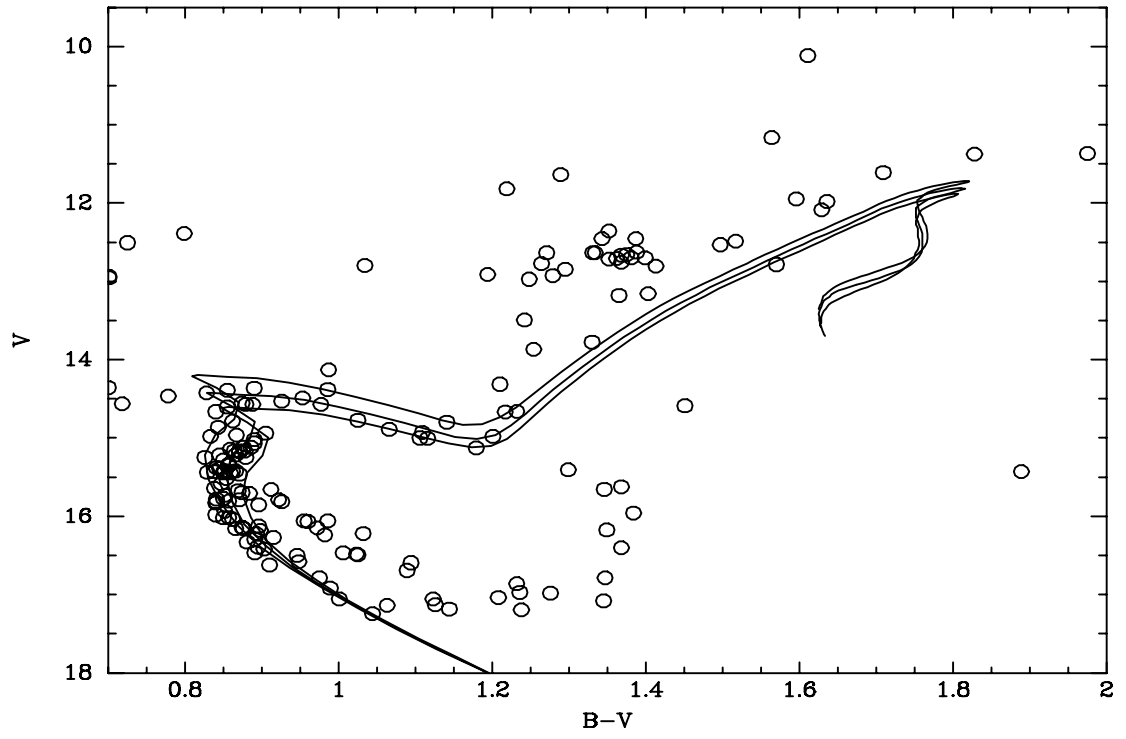


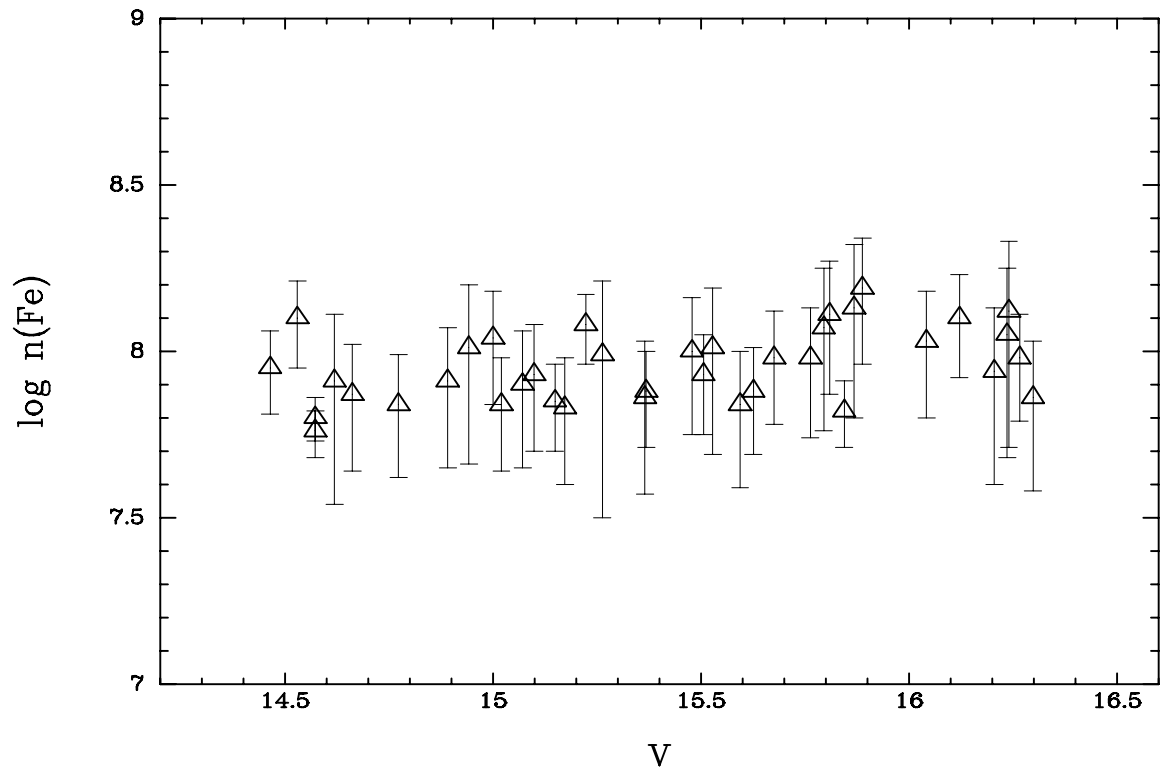












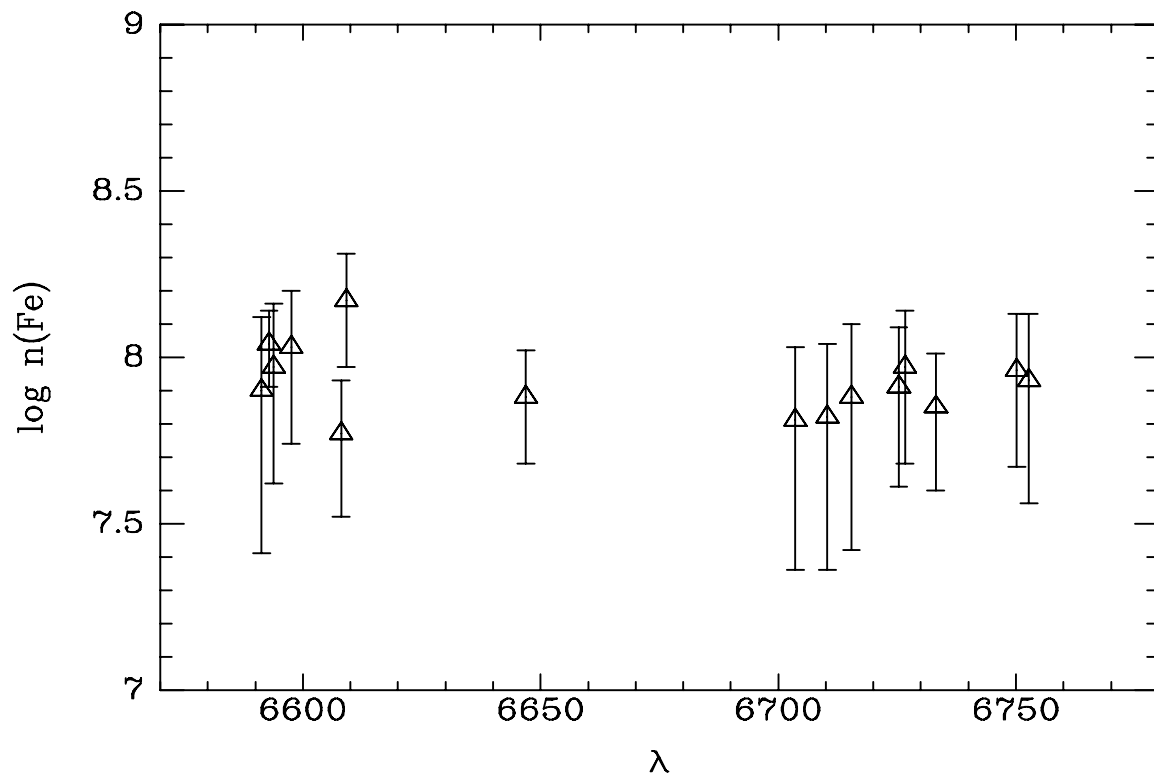


Table 1. NGC 6253 Star Identifications and Radial Velocities

| WEBDA ID | V_{rad} | $\sigma(V_r)$ | Num. | V | V_{Mo} | $B - V$ | $B - V_{Mo}$ | RVmem | S/N | $P(\mu)$ | Memb |
|----------|-----------|---------------|------|-------|----------|---------|--------------|-------|-----|----------|------|
| 7019 | -13.78 | 3.75 | 1 | 11.34 | ... | 0.33 | ... | nm | 97 | ... | NM |
| 1760 | -27.89 | 1.42 | 1 | 11.37 | ... | 1.98 | ... | m | 24 | ... | M |
| 7020 | -49.43 | 1.25 | 1 | 11.38 | ... | 1.83 | ... | nm | 22 | ... | NM |
| 1492 | -31.75 | 0.95 | 1 | 11.61 | ... | 1.71 | ... | m | 24 | ... | M |
| 7023 | -29.61 | 0.90 | 1 | 11.95 | ... | 1.60 | ... | m | 25 | ... | M |
| 7024 | -21.95 | 1.36 | 1 | 11.97 | ... | 0.47 | ... | nm | 127 | ... | NM |
| 7025 | -29.58 | 0.87 | 1 | 11.98 | ... | 1.64 | ... | m | 23 | ... | M |
| 7027 | 4.59 | 0.87 | 1 | 12.09 | ... | 1.63 | ... | nm | 27 | ... | NM |
| 5201 | -24.25 | 5.52 | 1 | 12.14 | 12.148 | 0.48 | 0.492 | nm? | 82 | 85 | M? |
| 3595 | -28.93 | 1.21 | 1 | 12.35 | 12.360 | 1.35 | 1.252 | m | 28 | 93 | M |
| 7028 | 3.73 | 0.99 | 1 | 12.46 | ... | 1.39 | ... | nm | 42 | ... | NM |
| 7029 | -28.52 | 1.15 | 1 | 12.46 | ... | 1.34 | ... | m | 27 | ... | M |
| 7030 | -57.68 | 0.71 | 1 | 12.49 | 12.502 | 1.52 | 1.440 | nm | 45 | ... | NM |
| 7031 | -54.29 | 1.90 | 1 | 12.51 | 12.390 | 0.73 | 0.872 | nm | 48 | ... | NM |
| 2541 | -29.93 | 0.84 | 1 | 12.53 | 12.553 | 1.50 | 1.372 | m | 28 | 79 | M |
| 2885 | -29.01 | 1.01 | 1 | 12.63 | 12.629 | 1.39 | 1.289 | m | 28 | 91 | M |
| 7032 | -31.22 | 1.06 | 1 | 12.64 | 12.638 | 1.33 | 1.255 | m | 27 | 80 | M |
| 7033 | -28.83 | 1.10 | 1 | 12.66 | ... | 1.38 | ... | m | 27 | ... | M |
| 7034 | -28.83 | 1.06 | 1 | 12.70 | 12.642 | 1.38 | 1.300 | m | 26 | ... | M |
| 7035 | 5.28 | 1.17 | 1 | 12.70 | 12.656 | 1.40 | 1.320 | nm | 33 | ... | NM |
| 4510 | -27.48 | 1.05 | 1 | 12.71 | 12.713 | 1.36 | 1.268 | m | 32 | 91 | M |
| 7037 | -30.71 | 1.01 | 1 | 12.76 | 12.755 | 1.37 | 1.290 | m | 30 | 69 | M |
| 7038 | 40.95 | 9.03 | 1 | 12.77 | 12.717 | 0.36 | 0.412 | nm | 49 | ... | NM |
| 7040 | -27.50 | 0.89 | 1 | 12.79 | ... | 1.57 | ... | m | 24 | ... | M |
| 7042 | -30.07 | 1.16 | 1 | 12.81 | 12.811 | 1.41 | 1.310 | m | 27 | 61 | M |
| 7043 | -73.72 | 1.15 | 1 | 12.85 | 12.821 | 1.30 | 1.295 | nm | 33 | 27 | NM |
| 7044 | -52.93 | 1.33 | 1 | 12.86 | 12.782 | 0.62 | 0.675 | nm | 65 | ... | NM |
| 7045 | -32.97 | 0.81 | 1 | 12.91 | 12.854 | 1.19 | 1.136 | m | 46 | ... | M |
| 2027 | -1.98 | 1.55 | 1 | 12.94 | 12.931 | 0.70 | 0.691 | nm | 79 | 42 | NM |
| 7048 | 0.37 | 0.78 | 1 | 12.97 | 12.930 | 1.25 | 1.200 | nm | 49 | ... | NM |
| 2269 | -28.96 | 1.37 | 1 | 13.16 | 13.162 | 1.40 | 1.294 | m | 28 | 95 | M |
| 2542 | -24.52 | 1.27 | 1 | 13.18 | 13.175 | 1.37 | 1.269 | nm? | 29 | 94 | M? |
| 3138 | -31.17 | 0.83 | 1 | 13.50 | 13.501 | 1.24 | 1.144 | m | 36 | 97 | M |
| 2126 | -37.14 | 1.79 | 1 | 13.54 | 13.516 | 0.63 | 0.642 | nm | 50 | 95 | M?BS |
| 2568 | -58.66 | 1.61 | 1 | 13.78 | 13.799 | 1.33 | 1.253 | nm | 39 | 95 | NM |
| 3168 | -29.95 | 32.26 | 3 | 14.36 | 14.363 | 0.89 | 0.688 | varVr | 145 | 98 | M |
| 2507 | -37.11 | 17.65 | 3 | 14.43 | 14.405 | 0.83 | 0.776 | varVr | 113 | 97 | M |
| 1741 | -28.88 | 0.17 | 2 | 14.46 | ... | 0.78 | ... | m | 106 | ... | M |
| 2561 | -30.29 | 0.54 | 4 | 14.53 | ... | 0.93 | ... | m | 66 | ... | M |
| 2193 | -27.01 | 4.84 | 4 | 14.56 | ... | 0.72 | ... | m | 171 | ... | M |
| 2864 | -32.24 | 0.53 | 4 | 14.57 | 14.579 | 0.98 | 0.906 | m | 99 | 92 | M |
| 7156 | -28.13 | 0.21 | 4 | 14.62 | 14.570 | 0.87 | 0.869 | m | 136 | ... | M |
| 2131 | -30.73 | 4.86 | 4 | 14.66 | 14.668 | 0.85 | 0.813 | m | 146 | 92 | M |
| 2562 | -28.84 | 0.38 | 4 | 14.66 | 14.665 | 1.23 | 1.134 | m | 45 | 97 | M |
| 3212 | -5.54 | 0.34 | 3 | 14.69 | 14.692 | 0.69 | 0.669 | nm | 145 | ... | NM |

Table 1—Continued

| WEBDA ID | V_{rad} | $\sigma(V_r)$ | Num. | V | V_{Mo} | $B - V$ | $B - V_{Mo}$ | RVmem | S/N | $P(\mu)$ | Memb |
|----------|-----------|---------------|------|-------|----------|---------|--------------|-------|-----|----------|------|
| 1172 | -29.63 | 0.12 | 4 | 14.77 | 14.783 | 1.03 | 0.941 | m | 100 | 93 | M |
| 1704 | -29.26 | 0.67 | 4 | 14.89 | 14.885 | 1.07 | 0.966 | m | 80 | 96 | M |
| 1562 | -29.82 | 2.28 | 3 | 14.94 | 14.939 | 0.91 | 0.855 | m | 131 | 95 | M |
| 1311 | -29.04 | 0.39 | 4 | 15.00 | 15.007 | 1.11 | 1.015 | m | 68 | 94 | M |
| 1888 | -30.72 | 4.03 | 4 | 15.02 | 15.033 | 0.89 | 0.840 | m | 124 | 94 | M |
| 7255 | -29.31 | 0.62 | 4 | 15.07 | 15.085 | 0.87 | 0.836 | m | 118 | 93 | M |
| 7267 | -30.35 | 2.89 | 4 | 15.10 | ... | 0.85 | ... | m | 128 | ... | M |
| 4735 | -27.36 | 1.63 | 4 | 15.15 | 15.178 | 0.87 | 0.829 | m | 121 | 94 | M |
| 7284 | -27.85 | 0.38 | 4 | 15.17 | ... | 0.88 | ... | m | 131 | ... | M |
| 3248 | -55.08 | 1.94 | 3 | 15.19 | 15.187 | 0.68 | 0.664 | nm | 132 | 3 | NM |
| 7292 | -29.28 | 1.41 | 4 | 15.22 | 15.231 | 0.83 | 0.826 | m | 117 | 85 | M |
| 7300 | -29.19 | 0.49 | 2 | 15.26 | 15.232 | 0.87 | 0.854 | m | 84 | ... | M |
| 7303 | -18.38 | 16.42 | 3 | 15.27 | 15.235 | 0.84 | 0.850 | varVr | 101 | ... | M |
| 7329 | -29.16 | 0.27 | 4 | 15.37 | 15.329 | 0.88 | 0.903 | m | 82 | ... | M |
| 596 | -29.13 | 0.87 | 3 | 15.37 | 13.379 | 0.85 | 0.793 | m | 110 | 94 | M |
| 7348 | -36.63 | 1.65 | 3 | 15.43 | 15.423 | 0.82 | 0.791 | nm | 127 | 93 | M? |
| 7370 | -28.95 | 0.81 | 4 | 15.48 | 15.476 | 0.87 | 0.841 | m | 91 | 85 | M |
| 7377 | -28.70 | 0.88 | 4 | 15.51 | 15.532 | 0.83 | 0.788 | m | 93 | ... | M |
| 7390 | -30.90 | 0.96 | 4 | 15.53 | 15.495 | 0.82 | 0.834 | m | 93 | ... | M |
| 3141 | -28.81 | 0.12 | 4 | 15.59 | 15.603 | 0.87 | 0.827 | m | 104 | 83 | M |
| 7427 | -30.51 | 0.60 | 4 | 15.63 | 15.592 | 0.86 | 0.858 | m | 91 | ... | M |
| 3643 | -30.77 | 1.03 | 4 | 15.68 | 15.679 | 0.86 | 0.830 | m | 108 | 79 | M |
| 7448 | -62.90 | 0.37 | 3 | 15.68 | 15.672 | 0.85 | 0.847 | nm | 94 | 63 | NM |
| 7470 | -29.73 | 3.24 | 4 | 15.76 | 15.738 | 0.88 | 0.873 | m | 93 | ... | M |
| 4293 | -29.21 | 1.54 | 4 | 15.80 | 15.797 | 0.86 | 0.831 | m | 78 | 91 | M |
| 7486 | -28.85 | 0.13 | 3 | 15.81 | 15.829 | 0.82 | 0.788 | m | 89 | 86 | M |
| 7495 | -51.96 | 19.51 | 3 | 15.84 | 15.814 | 0.84 | 0.825 | varVr | 101 | ... | M |
| 1474 | -29.51 | 0.82 | 4 | 15.84 | 15.857 | 0.88 | 0.825 | m | 114 | 91 | M |
| 7505 | -31.27 | 1.01 | 4 | 15.87 | 15.893 | 0.87 | 0.819 | m | 65 | 88 | M |
| 7511 | -28.93 | 0.65 | 4 | 15.89 | 15.906 | 0.84 | 0.810 | m | 68 | 87 | M |
| 7584 | -29.81 | 0.66 | 4 | 16.04 | 16.043 | 0.87 | 0.834 | m | 79 | 90 | M |
| 7592 | -27.38 | 10.03 | 3 | 16.05 | 16.040 | 0.86 | 0.856 | varVr | 72 | ... | M |
| 7627 | -29.97 | 1.33 | 4 | 16.12 | 16.082 | 0.87 | 0.870 | m | 71 | ... | M |
| 7638 | -28.19 | 0.48 | 3 | 16.16 | 16.165 | 0.88 | 0.829 | m | 77 | 3 | NM |
| 7662 | -41.90 | 0.21 | 2 | 16.20 | 16.201 | 0.88 | 0.855 | nm | 75 | 30 | NM |
| 7664 | -29.01 | 0.99 | 4 | 16.21 | 16.221 | 0.90 | 0.854 | m | 77 | 87 | M |
| 7672 | 23.42 | 0.48 | 3 | 16.22 | 16.298 | 0.93 | 0.825 | nm | 74 | 86 | NM |
| 1691 | -28.77 | 0.44 | 4 | 16.24 | 16.249 | 0.89 | 0.849 | m | 72 | 51 | M |
| 7676 | -30.35 | 1.07 | 4 | 16.24 | 16.241 | 0.85 | 0.840 | m | 45 | 54 | M |
| 7694 | -27.60 | 3.30 | 4 | 16.27 | 16.279 | 0.88 | 0.855 | m | 83 | 77 | M |
| 7718 | -25.39 | 0.79 | 4 | 16.30 | 16.322 | 0.93 | 0.841 | m | 70 | ... | M |
| 7720 | 51.48 | 0.72 | 3 | 16.30 | 16.314 | 0.93 | 0.882 | nm | 76 | ... | NM |
| 7806 | -30.23 | 1.03 | 4 | 16.45 | 16.470 | 0.89 | 0.852 | m | 57 | ... | NM |
| 7822 | -29.94 | 0.33 | 3 | 16.49 | 16.496 | 0.91 | 0.865 | m | 34 | 80 | M |

Note. — S/N refers to the ratio of signal to noise per pixel; *m* refers to probable member single stars; *nm* may include both probable non-members and undetected binaries.

Table 2. Measured Equivalent Widths for MS/TO Stars

| WEBDA ID | Fe lines (λ in \AA) | | | | | | | | | | | | | | | | Nickel lines | | Ca line | Si line |
|------------|----------------------------------------|--------|--------|--------|--------|--------|--------|--------|--------|--------|--------|--------|--------|--------|--------|--------|--------------|--------|---------|---------|
| Wavelength | 6591.3 | 6592.9 | 6593.9 | 6597.6 | 6608.0 | 6609.1 | 6646.9 | 6703.6 | 6710.3 | 6715.4 | 6725.4 | 6726.7 | 6733.1 | 6750.2 | 6572.7 | 6643.6 | 6767.8 | 6772.3 | 6717.7 | 6721.8 |
| Exc. Pot | 4.59 | 2.73 | 2.43 | 4.79 | 2.28 | 2.56 | 2.61 | 2.76 | 1.48 | 4.61 | 4.10 | 4.61 | 4.64 | 2.42 | 4.64 | 1.68 | 1.83 | 3.66 | 2.71 | 5.86 |
| $\log gf$ | -1.81 | -1.30 | -2.23 | -0.90 | -3.93 | -2.57 | -3.87 | -2.98 | -4.71 | -1.38 | -2.16 | -1.03 | -1.33 | -2.65 | -1.18 | -1.92 | -2.02 | -0.86 | -0.26 | -1.07 |
| 1741 | 23.1 | 153.4 | 109.3 | 67.2 | 26.4 | 92.4 | 18.1 | 36.9 | ... | 37.0 | 19.3 | 60.9 | 41.6 | 93.1 | 43.3 | 123.3 | 89.6 | 62.8 | 148.2 | 65.7 |
| 2561 | 50.6 | ... | 129.0 | 72.5 | 57.9 | ... | 42.1 | 72.7 | ... | 71.1 | 44.1 | 81.6 | 50.2 | 104.4 | ... | 161.8 | 126.4 | 87.0 | ... | 80.6 |
| 2193 | ... | 127.1 | 83.5 | 47.1 | ... | 66.6 | ... | 33.8 | ... | 25.2 | 19.7 | 48.6 | 28.6 | 66.0 | 42.2 | 94.1 | 81.3 | 50.6 | 123.2 | 61.5 |
| 2864 | 30.9 | ... | 123.5 | 68.7 | 40.3 | ... | 28.1 | 58.2 | 42.9 | 54.0 | 36.6 | 71.4 | 46.2 | 96.4 | 63.0 | 134.5 | 109.1 | 73.3 | 166.7 | 73.4 |
| 7156 | 17.0 | 173.2 | 102.8 | 62.6 | 33.1 | 114.6 | 16.6 | 53.6 | 28.3 | 51.1 | 24.5 | 66.2 | 40.8 | 85.3 | 54.9 | 125.8 | 102.3 | 71.8 | 159.5 | 73.0 |
| 2131 | 21.3 | 157.4 | 110.9 | 62.3 | ... | 103.0 | ... | 50.5 | 26.7 | 35.1 | 22.9 | 53.1 | 44.2 | 89.8 | 51.0 | 116.7 | 106.8 | 67.1 | 153.8 | 76.2 |
| 1172 | ... | ... | 125.9 | 69.6 | 36.2 | 117.6 | 27.5 | 65.0 | 51.1 | 58.4 | 37.1 | 70.7 | 45.9 | 102.5 | 66.4 | 147.7 | 113.3 | 82.3 | 172.8 | 67.1 |
| 1704 | ... | 195.6 | 129.0 | 69.8 | 40.1 | 124.7 | 33.6 | 73.3 | 52.4 | 66.6 | 44.6 | 78.3 | 43.8 | 102.0 | 68.7 | 131.4 | 116.8 | 83.7 | 175.0 | 66.4 |
| 1562 | ... | ... | ... | ... | 18.9 | 112.6 | ... | 58.2 | 43.7 | 47.0 | ... | 80.2 | 58.9 | 90.9 | 55.3 | 122.9 | 113.4 | 73.5 | 169.5 | 77.4 |
| 1311 | 46.9 | ... | 147.2 | 78.5 | 46.8 | 127.4 | 41.0 | 75.9 | 70.8 | 70.4 | 46.0 | 78.8 | 53.8 | 117.5 | 84.2 | 151.2 | 127.2 | 78.1 | 189.7 | 69.8 |
| 1888 | 20.9 | 174.3 | 108.4 | 55.6 | 23.7 | 93.4 | ... | 41.2 | 23.1 | 40.6 | 33.5 | 65.4 | 37.5 | 85.6 | 57.2 | 118.2 | 100.4 | 65.8 | 156.0 | 64.1 |
| 7255 | 26.1 | 156.9 | 110.4 | 67.5 | 22.4 | 104.3 | ... | 43.3 | 23.1 | 48.0 | 32.9 | 66.5 | 43.3 | 80.3 | 55.4 | 121.0 | 106.1 | 70.3 | 160.0 | 77.9 |
| 7267 | 17.0 | 168.3 | 112.1 | 73.4 | 25.9 | 97.9 | ... | 41.2 | 26.7 | 40.8 | 31.8 | 66.8 | 31.8 | 89.3 | 47.4 | 116.5 | 96.1 | 67.2 | 146.4 | 75.1 |
| 4735 | 24.8 | 162.4 | 110.1 | 61.9 | 23.6 | 89.0 | 16.4 | 46.4 | 23.9 | 33.7 | 20.9 | 53.7 | 42.0 | 88.8 | 52.3 | 109.0 | 95.7 | 67.3 | 146.5 | 66.4 |
| 7284 | 17.7 | 155.1 | 92.0 | 67.4 | 19.3 | 95.9 | ... | 40.1 | 21.3 | 37.1 | 25.6 | 59.4 | 43.8 | 87.5 | 55.1 | 114.3 | 98.5 | 63.7 | 149.1 | 73.8 |
| 7292 | ... | 164.9 | 117.1 | 72.5 | ... | 80.5 | ... | 51.6 | 24.6 | 47.9 | 38.0 | 67.1 | ... | 86.0 | 56.4 | 121.6 | 92.2 | 69.5 | 173.0 | 81.9 |
| 7300 | 20.6 | 152.1 | 90.6 | 71.5 | 27.4 | 111.6 | ... | 47.7 | 28.2 | 47.2 | 29.0 | 53.6 | 41.1 | 96.7 | 62.8 | 125.1 | 121.0 | 82.7 | 161.3 | 82.0 |
| 7329 | 23.4 | 143.0 | 112.0 | 67.9 | 31.9 | 97.8 | ... | 46.0 | 17.3 | 32.0 | 24.1 | 52.2 | 33.2 | 83.9 | 58.5 | 112.0 | 98.0 | 69.0 | 145.9 | 70.2 |
| 596 | ... | 149.8 | 104.5 | 58.5 | 18.3 | 86.6 | ... | 43.0 | 29.1 | 27.8 | 25.3 | 56.5 | 43.8 | 92.7 | 50.4 | 113.8 | 97.4 | 70.8 | 145.2 | 65.9 |
| 7370 | ... | 168.4 | 120.8 | 52.7 | 22.0 | 96.4 | 19.8 | 45.7 | 17.0 | 51.8 | 28.5 | 71.5 | 58.9 | 94.0 | 59.3 | 121.6 | 83.3 | 67.1 | 148.7 | 73.0 |
| 7377 | ... | 161.3 | 93.1 | 61.4 | 15.5 | 80.0 | ... | 46.6 | ... | 50.8 | 25.2 | 68.6 | 43.5 | 70.5 | 46.5 | 103.4 | 96.9 | 58.9 | 143.2 | 66.5 |
| 7390 | ... | 142.2 | 121.6 | 55.5 | 24.3 | 97.8 | 20.7 | 41.1 | 16.0 | 54.0 | 27.9 | 66.3 | 39.4 | 76.0 | 50.9 | 103.3 | 91.1 | 83.7 | 142.0 | 59.2 |
| 3141 | 25.9 | 151.4 | 98.0 | 71.8 | 20.5 | 85.8 | ... | 37.1 | ... | 25.8 | 27.2 | 47.9 | 45.1 | 85.0 | 43.2 | 110.8 | 96.0 | 76.9 | 152.2 | 71.4 |
| 7247 | ... | 155.5 | 91.5 | 65.6 | 24.7 | 86.3 | ... | 38.8 | 21.1 | 37.1 | 33.2 | 66.2 | 26.4 | 80.6 | 46.3 | 116.1 | 95.2 | 57.9 | 139.1 | 73.1 |
| 3643 | 19.3 | 158.3 | 110.6 | 62.4 | 19.5 | 93.2 | 19.9 | 48.7 | 23.9 | 36.8 | 43.6 | 64.6 | 55.4 | 85.1 | 56.0 | 108.9 | 93.8 | 66.9 | 151.4 | 70.7 |
| 7470 | ... | 151.6 | 105.6 | 74.5 | 29.9 | ... | 15.3 | 47.6 | 19.9 | 45.8 | 45.2 | 79.5 | 52.1 | 96.1 | 52.6 | 120.8 | 113.3 | 70.5 | 160.9 | 74.7 |
| 4293 | 30.6 | 181.0 | 115.1 | 63.1 | 26.3 | 94.4 | 17.9 | 42.4 | 54.3 | 40.5 | 27.3 | 48.7 | 48.1 | 97.6 | 52.3 | 118.2 | 96.4 | 78.3 | 160.5 | 65.1 |
| 7486 | ... | 173.6 | 90.6 | 80.0 | 20.5 | 85.1 | ... | 55.3 | 23.1 | 36.7 | 36.6 | 80.9 | 52.4 | 84.3 | 46.4 | 113.0 | 112.6 | 57.6 | 147.8 | 89.7 |
| 1474 | ... | 152.1 | 93.8 | 58.2 | 21.0 | 83.3 | 16.9 | 48.3 | 27.5 | 33.1 | 20.9 | 62.1 | 41.2 | 82.5 | 52.0 | 119.7 | 101.6 | 64.7 | 151.8 | 69.1 |
| 7505 | ... | 156.3 | 87.4 | 62.5 | 21.9 | 97.8 | ... | 75.0 | 24.5 | 54.4 | 37.6 | 90.4 | 55.9 | 99.4 | 73.3 | 137.7 | 85.3 | 85.3 | 139.2 | 86.0 |
| 7511 | 48.5 | 166.2 | 131.6 | 77.5 | ... | ... | ... | 63.1 | 38.6 | 41.2 | 38.5 | 68.8 | 50.0 | 85.6 | 55.1 | 113.0 | 123.2 | 83.3 | 156.9 | 104.4 |
| 7584 | 19.3 | 174.6 | 95.6 | 81.0 | ... | 89.0 | 16.2 | 58.1 | 22.7 | 45.1 | 32.7 | 74.1 | 43.7 | 95.8 | 50.1 | 127.8 | 90.3 | 71.5 | 181.3 | 72.1 |
| 7627 | ... | 167.7 | 104.6 | 68.8 | 28.3 | 82.7 | 29.1 | 54.7 | 40.8 | 49.0 | 41.6 | 70.9 | 56.7 | 97.0 | 78.8 | 119.0 | 99.3 | 72.1 | 157.0 | 77.8 |
| 7664 | 28.6 | 175.2 | 97.2 | 78.9 | 26.0 | ... | ... | 48.5 | 36.8 | 68.0 | 23.0 | 65.7 | 38.0 | 76.7 | 52.7 | 124.3 | 94.7 | 84.4 | 147.7 | 58.1 |
| 1691 | ... | 163.0 | 118.3 | 91.9 | 32.7 | 86.8 | 16.2 | 41.4 | 16.9 | 52.1 | 54.3 | 77.9 | 50.6 | 91.8 | 55.5 | 131.4 | 102.1 | 60.5 | 175.2 | 85.7 |
| 7676 | ... | 133.6 | ... | 81.3 | 20.6 | 77.6 | 18.8 | 65.9 | 27.9 | 71.1 | ... | 62.5 | ... | 105.5 | 50.9 | 142.6 | 117.9 | 67.0 | 154.6 | 58.4 |
| 7694 | 21.7 | 175.8 | 109.4 | 72.9 | 40.0 | ... | 18.2 | 55.6 | 19.9 | 29.3 | 44.3 | 71.7 | 57.5 | 83.1 | 55.8 | 129.7 | 95.4 | 72.7 | 132.3 | 62.1 |
| 7718 | ... | 156.9 | 110.4 | 67.5 | 22.4 | 104.3 | ... | 43.3 | 23.1 | 48.0 | 32.9 | 66.5 | 43.3 | 80.3 | 55.4 | 121.0 | 106.1 | 70.3 | 160.0 | 77.9 |

Note. — Equivalent widths are expressed in milliÅngstroms ($m\text{\AA}$), excitation potentials in electron volts.

Table 3. Abundances for TO/MS Stars in NGC 6253

| WEBDA ID | [Fe/H] | <i>s</i> + | <i>s</i> − | No. lines | Ni | <i>s</i> + | <i>s</i> − | Ca | σ | Si | σ | T_{eff} | log <i>g</i> | V_t |
|----------|--------|------------|------------|-----------|------|------------|------------|------|----------|------|----------|-----------|--------------|-------|
| 1741 | 0.43 | 0.03 | 0.04 | 14 | 0.42 | 0.12 | 0.16 | 0.69 | 0.06 | 0.34 | 0.06 | 6208 | 3.82 | 1.50 |
| 2561 | 0.58 | 0.04 | 0.04 | 11 | 0.80 | 0.10 | 0.13 | ... | ... | 0.50 | 0.09 | 5724 | 3.74 | 1.22 |
| 2193 | 0.24 | 0.02 | 0.02 | 11 | 0.21 | 0.01 | 0.01 | 0.42 | 0.05 | 0.34 | 0.04 | 6421 | 3.82 | 1.67 |
| 2864 | 0.28 | 0.02 | 0.02 | 13 | 0.37 | 0.07 | 0.08 | 0.60 | 0.04 | 0.41 | 0.06 | 5572 | 3.72 | 1.12 |
| 7156 | 0.39 | 0.06 | 0.07 | 15 | 0.39 | 0.06 | 0.07 | 0.69 | 0.04 | 0.40 | 0.04 | 5913 | 3.77 | 1.33 |
| 2131 | 0.35 | 0.05 | 0.05 | 13 | 0.41 | 0.04 | 0.05 | 0.66 | 0.04 | 0.45 | 0.05 | 5975 | 3.84 | 1.29 |
| 1172 | 0.32 | 0.05 | 0.05 | 13 | 0.51 | 0.08 | 0.09 | 0.58 | 0.03 | 0.34 | 0.06 | 5435 | 3.71 | 1.02 |
| 1704 | 0.39 | 0.05 | 0.06 | 14 | 0.40 | 0.04 | 0.05 | 0.53 | 0.04 | 0.36 | 0.08 | 5323 | 3.70 | 0.95 |
| 1562 | 0.49 | 0.08 | 0.09 | 9 | 0.50 | 0.04 | 0.04 | 0.73 | 0.04 | 0.47 | 0.06 | 5789 | 3.89 | 1.07 |
| 1311 | 0.52 | 0.04 | 0.05 | 14 | 0.54 | 0.05 | 0.06 | 0.57 | 0.04 | 0.45 | 0.09 | 5218 | 3.70 | 0.86 |
| 1888 | 0.32 | 0.04 | 0.05 | 14 | 0.36 | 0.05 | 0.05 | 0.63 | 0.04 | 0.28 | 0.05 | 5837 | 3.90 | 1.10 |
| 7255 | 0.38 | 0.05 | 0.06 | 14 | 0.48 | 0.04 | 0.04 | 0.70 | 0.04 | 0.48 | 0.05 | 5897 | 3.92 | 1.12 |
| 7267 | 0.41 | 0.05 | 0.05 | 14 | 0.39 | 0.05 | 0.06 | 0.58 | 0.04 | 0.45 | 0.05 | 5952 | 3.94 | 1.14 |
| 4735 | 0.33 | 0.03 | 0.04 | 15 | 0.34 | 0.01 | 0.01 | 0.56 | 0.05 | 0.32 | 0.05 | 5910 | 3.97 | 1.07 |
| 7284 | 0.31 | 0.05 | 0.05 | 14 | 0.38 | 0.05 | 0.05 | 0.58 | 0.04 | 0.43 | 0.05 | 5881 | 3.98 | 1.03 |
| 7292 | 0.56 | 0.03 | 0.03 | 11 | 0.52 | 0.09 | 0.12 | 0.88 | 0.03 | 0.55 | 0.06 | 6038 | 4.03 | 1.09 |
| 7300 | 0.47 | 0.07 | 0.09 | ... | 0.76 | 0.05 | 0.06 | 0.71 | 0.05 | 0.54 | 0.08 | 5910 | 4.02 | 1.00 |
| 7329 | 0.34 | 0.06 | 0.06 | 14 | 0.44 | 0.01 | 0.01 | 0.52 | 0.06 | 0.39 | 0.07 | 5859 | 4.07 | 0.90 |
| 596 | 0.36 | 0.04 | 0.04 | 13 | 0.49 | 0.03 | 0.03 | 0.57 | 0.04 | 0.33 | 0.06 | 5971 | 4.07 | 0.99 |
| 7370 | 0.48 | 0.05 | 0.06 | 14 | 0.51 | 0.12 | 0.16 | 0.56 | 0.05 | 0.43 | 0.06 | 5894 | 4.11 | 0.87 |
| 7377 | 0.41 | 0.04 | 0.05 | 12 | 0.40 | 0.06 | 0.07 | 0.57 | 0.05 | 0.34 | 0.07 | 6021 | 4.12 | 0.96 |
| 7390 | 0.49 | 0.06 | 0.07 | 14 | 0.61 | 0.12 | 0.17 | 0.57 | 0.05 | 0.25 | 0.06 | 6055 | 4.13 | 0.97 |
| 3141 | 0.32 | 0.05 | 0.06 | 13 | 0.54 | 0.05 | 0.06 | 0.58 | 0.04 | 0.41 | 0.05 | 5888 | 4.16 | 0.80 |
| 7427 | 0.36 | 0.04 | 0.05 | 13 | 0.48 | 0.09 | 0.11 | 0.47 | 0.05 | 0.43 | 0.07 | 5920 | 4.17 | 0.81 |
| 3643 | 0.46 | 0.04 | 0.04 | 15 | 0.46 | 0.02 | 0.02 | 0.59 | 0.04 | 0.40 | 0.05 | 5926 | 4.18 | 0.81 |
| 7470 | 0.46 | 0.05 | 0.06 | 13 | 0.65 | 0.07 | 0.08 | 0.62 | 0.04 | 0.45 | 0.06 | 5865 | 4.21 | 0.80 |
| 4293 | 0.55 | 0.06 | 0.06 | 15 | 0.63 | 0.05 | 0.06 | 0.66 | 0.04 | 0.32 | 0.08 | 5932 | 4.21 | 0.80 |
| 7486 | 0.59 | 0.05 | 0.06 | 13 | 0.69 | 0.12 | 0.17 | 0.62 | 0.05 | 0.66 | 0.07 | 6061 | 4.22 | 0.86 |
| 1474 | 0.30 | 0.03 | 0.03 | 14 | 0.54 | 0.06 | 0.08 | 0.54 | 0.03 | 0.37 | 0.05 | 5874 | 4.23 | 0.80 |
| 7505 | 0.61 | 0.06 | 0.07 | 13 | 0.75 | 0.12 | 0.17 | 0.43 | 0.06 | 0.59 | 0.11 | 5894 | 4.24 | 0.80 |
| 7511 | 0.67 | 0.05 | 0.06 | 12 | 0.85 | 0.10 | 0.12 | 0.66 | 0.05 | 0.88 | 0.08 | 5995 | 4.24 | 0.80 |
| 7584 | 0.51 | 0.05 | 0.05 | 14 | 0.62 | 0.10 | 0.13 | 0.77 | 0.04 | 0.41 | 0.07 | 5910 | 4.27 | 0.80 |
| 7627 | 0.58 | 0.04 | 0.04 | 14 | 0.58 | 0.03 | 0.04 | 0.59 | 0.05 | 0.48 | 0.09 | 5913 | 4.28 | 0.80 |
| 7638 | 0.44 | 0.06 | 0.06 | 15 | 0.60 | 0.06 | 0.08 | 0.46 | 0.05 | 0.95 | 0.10 | 5872 | 4.29 | 0.80 |
| 7664 | 0.42 | 0.06 | 0.07 | 13 | 0.61 | 0.09 | 0.11 | 0.43 | 0.04 | 0.21 | 0.07 | 5811 | 4.30 | 0.80 |
| 1691 | 0.53 | 0.06 | 0.08 | 14 | 0.59 | 0.11 | 0.15 | 0.67 | 0.05 | 0.58 | 0.08 | 5849 | 4.31 | 0.80 |
| 7676 | 0.60 | 0.08 | 0.09 | 11 | 0.89 | 0.10 | 0.14 | 0.59 | 0.08 | 0.22 | 0.13 | 5971 | 4.31 | 0.80 |
| 7694 | 0.46 | 0.04 | 0.05 | 14 | 0.61 | 0.08 | 0.10 | 0.30 | 0.05 | 0.27 | 0.07 | 5856 | 4.31 | 0.80 |
| 7718 | 0.34 | 0.06 | 0.06 | 13 | 0.49 | 0.03 | 0.03 | 0.46 | 0.05 | 0.47 | 0.08 | 5725 | 4.32 | 0.80 |
| 7806 | 0.63 | 0.05 | 0.06 | 12 | 0.70 | 0.06 | 0.08 | 0.58 | 0.06 | 0.22 | 0.08 | 5849 | 4.35 | 0.80 |

Table 4. Iron Abundances from synthesis for RG Members

| WEBDA ID | [Fe/H] | σ | N(λ) | T_{eff} | log g | V_t |
|----------|--------|----------|----------------|-----------|---------|-------|
| 3595 | 0.46 | 0.04 | 7 | 4676 | 2.34 | 1.53 |
| 7029 | 0.46 | 0.04 | 6 | 4694 | 2.41 | 1.52 |
| 2541 | 0.49 | 0.02 | 7 | 4408 | 2.46 | 1.52 |
| 2885 | 0.46 | 0.06 | 7 | 4607 | 2.52 | 1.52 |
| 7032 | 0.45 | 0.03 | 6 | 4717 | 2.52 | 1.51 |
| 7033 | 0.46 | 0.04 | 7 | 4632 | 2.54 | 1.50 |
| 7034 | 0.46 | 0.04 | 6 | 4620 | 2.56 | 1.50 |
| 4510 | 0.48 | 0.04 | 7 | 4657 | 2.57 | 1.50 |
| 7037 | 0.40 | 0.07 | 7 | 4645 | 2.59 | 1.50 |
| 7040 | 0.46 | 0.06 | 4 | 4280 | 2.62 | 1.48 |
| 7042 | 0.49 | 0.02 | 7 | 4560 | 2.63 | 1.49 |
| 2269 | 0.46 | 0.04 | 6 | 4579 | 2.82 | 1.46 |
| 2542 | 0.43 | 0.06 | 6 | 4651 | 2.83 | 1.46 |
| 3138 | 0.41 | 0.04 | 6 | 4902 | 3.02 | 1.44 |
| 2562 | 0.45 | 0.03 | 6 | 4928 | 3.65 | 1.36 |

Table 5. Abundances by line, MS/TO stars

| λ | No. stars | [A/H] | s.e.m.+ | s.e.m.- | Solar EW (mÅ) |
|------------|-----------|-------|---------|---------|---------------|
| Iron lines | | | | | |
| 6591.3 | 20 | 0.36 | 0.07 | 0.08 | 16.4 |
| 6592.9 | 33 | 0.52 | 0.02 | 0.02 | 146.9 |
| 6593.9 | 36 | 0.44 | 0.04 | 0.04 | 98.4 |
| 6597.6 | 37 | 0.50 | 0.03 | 0.04 | 48.7 |
| 6608.0 | 33 | 0.26 | 0.03 | 0.04 | 21.2 |
| 6609.1 | 32 | 0.65 | 0.03 | 0.03 | 73.4 |
| 6646.9 | 19 | 0.36 | 0.04 | 0.04 | 13.0 |
| 6703.6 | 38 | 0.29 | 0.04 | 0.05 | 42.7 |
| 6710.3 | 33 | 0.30 | 0.05 | 0.05 | 22.3 |
| 6715.4 | 38 | 0.36 | 0.05 | 0.05 | 33.0 |
| 6725.4 | 36 | 0.38 | 0.04 | 0.04 | 20.8 |
| 6726.7 | 38 | 0.45 | 0.03 | 0.04 | 51.0 |
| 6733.1 | 36 | 0.33 | 0.03 | 0.03 | 33.8 |
| 6750.2 | 38 | 0.43 | 0.03 | 0.04 | 77.3 |
| 6752.7 | 37 | 0.40 | 0.03 | 0.04 | 41.7 |
| Calcium | | | | | |
| 6717.7 | 37 | 0.61 | 0.02 | 0.02 | 127.0 |
| Silicon | | | | | |
| 6721.8 | 38 | 0.43 | 0.03 | 0.03 | 48.8 |
| Nickel | | | | | |
| 6643.6 | 38 | 0.60 | 0.03 | 0.03 | 102.0 |
| 6767.8 | 38 | 0.50 | 0.04 | 0.04 | 88.3 |
| 6772.3 | 38 | 0.46 | 0.03 | 0.03 | 55.8 |